The Palaeobotanist 69(2020): 93–118
0031–0174/2020

Palaeoproterozoic (2.2 Ga) life on land near Medicine Bow Peak, Wyoming, U.S.A.

GREGORY J. RETALLACK

Department of Earth Sciences, University of Oregon, Eugene, Oregon 87403–1272, USA.
Email: gregr@uoregon.edu

(Received 02 December, 2020; revised version accepted 16 July, 2021)

ABSTRACT

Retallack GJ 2020. Palaeoproterozoic (2.2 Ga) life on land near Medicine Bow Peak, Wyoming, U.S.A. The Palaeobotanist 69(1–2): 93–118.

Tubular megafossils from the Palaeoproterozoic (*ca.* 2.3 Ga) Medicine Peak Quartzite of Wyoming have been regarded as possibly the earliest metazoan burrows. This interpretation has been controversial because these fossils are much older than accepted traces of metazoans. Additional similar specimens have now been found in palaeosols of the overlying Sugarloaf Quartzite (*ca.* 2.2 Ga), in the same area. These newly discovered fossils postdate fluvial deposition, predate metamorphic veining, and formed during oxidative, red, gypsic, soil formation. Oxidized tubular features lack regularity of width, backfills, scratches, or other complexities of metazoan trace fossils, and are more like cyanobacterial ropes, slime mold slugs, and fungal and lichen thalli of biological soil crusts. Because exact biological affinities are unknown, the fossils are assigned to palaeobotanical form taxa like many Precambrian fossils: *Erythronema ramosum* and *E. robustum* gen. et sp. nov. and *Koilosolos pravus* gen. et sp. nov. Such vertical, irregularly tubular fossils, which destroy prior bedding, are evidence of biological activity in Palaeoproterozoic palaeosols.

Key–words—Trace fossil, Palaeosol, Palaeoproterozoic, Wyoming.

मेडिसिन बो पीक, व्योमिंग, यू.एस.ए. के निकट भूमि पर पुराप्राग्जीव (2.2 Ga) जीवन

ग्रेगरी जे. रेटलक

सारांश

व्योमिंग के पुराप्राग्जीव (2.3 Ga) मेडिसिन पीड क्वार्टज़ाइट से नलिकाकार स्थूलजीवाश्म संभवतः प्राचीनतम उत्तरजंतु मांदा के रूप में माने गए हैं। यह विवेचन विवादास्पद रहा है क्योंकि ये जीवाश्म उत्तर जंतुओं के स्वीकृत अनुरेखकों की अपेक्षा अति प्राचीन हैं। इसी क्षेत्र में उपरिशायी सुगरलोफ क्वार्टज़ाइट (2.2 Ga) के पुरानिखातों में अतिरिक्त सदृश प्रतिदर्श अब मिले हैं। ये नूतन अन्वेषित जीवाश्म नदीय निक्षेपण को उत्तर दिनांकित, कायांतरित शिरायन पूर्व दिनांकित करते हैं तथा उपचायी, लाल, जिप्सिक, मृदा शैलसमूह के दौरान गठित हुए। ऑक्सीकृत नलिकाकार लक्षण, चौड़ाई पृष्ठभरण, खरोंच, या उत्तरजंतु अनुपथ जीवाश्मों की अन्य जटिलताओं की नियमितताओं की कमी करते हैं तथा सायनोबैक्टीरियाई रज्जु अवपंक फफूँदी स्लग, कवक तथा जैविक मृदा पर्पटी की लाइकैन थैलाई की तरह ज्यादा हैं। चूंकि यथार्थ जैविक बंधुताएं अज्ञात हैं, जीवाश्म पुरावनस्पति प्ररूप टैक्सा जैसी बहुत से कैंब्रियन पूर्व जीवाश्म : *ऐरीथ्रोनेमा रेमोसम* और *ई. रोबस्टम* वंश अन्य जाति नवम एवं *कोइलोसोलोज प्रवस* वंश अन्य जाति को नियत हैं। ऐसे लंबवत, अनियमित नलिकाकार जीवाश्म, जो पूर्व संस्तरण नष्ट करते हैं, तथा पुराप्राग्जीव पुरानिखातों में जैविक गतिविधि के प्रमाण हैं।

सूचक शब्द—अनुपथ जीवाश्म, पुरानिखात, पुराप्राग्जीव, व्योंमिंग।

INTRODUCTION

PUTATIVE trace fossils attributed to metazoans older than Ediacaran (> 635 Ma) have been controversial, because there is little supporting evidence for worms, or complex metazoans, so far back in time (Bengtson *et al.*, 2007; Gaidos *et al.*, 2007; Maloof *et al.*, 2010, 2011; Huldtgren *et al.*, 2011). Pre–Ediacaran megafossils preserved in sandstone are especially problematic (Table 1), unlike microbial textures in sandstones (Noffke *et al.,* 2006; Noffke, 2007), stromatolites

Table 1—Problematic pre–Ediacaran non–calcareous and non–carbonaceous megafossils.

Original name	Age (Ga)	Formation	Location	Original interpretation	Nature here advocated	References
frond–like fossils	0.7	Elatina Formation	Mt Remarkable, S. Australia	Vendobiont	Vendobiont	Runnegar & Fedonkin, 1991
Laionanella multicycla	0.7	Xingmincun Formation	Yangtun, China	Problematicum	Vendobiont	Zhang *et al.*, 2006
Circular remains	0.7	Maikhanuul Formation	Zavkhan, Mongolia	Microbial colony	Microbial colony	Serezhnikova *et al.*, 2014
Nimbia occlusal, Aspidella terranovica	0.8	Kurgan Formation	Lesser Karatau, Mongolia	Ediacara fossils	Microbial colony	Meert *et al.*, 2011
Discoid fossils	0.8	Nanguanling Formation	Southern Liaoning, China	Problematicum	Vendobiont	Zhang *et al.*, 2006
Beltanelliformis brunsae	0.8	Twitya Formation	Corn Creek, NWT, Canada	Vendobiont	Vendobiont	Narbonne *et al.*, 1994
disc–shaped fossils	0.8	Alwar Quartzite	Ferozpur Jhirka, India	Vendobiont	Vendobiont	Hofmann, 1991a
cf *Dickinsonia costata*	0.8	Liulaobai Formation	Liulaobai, China	Vendobiont	Vendobiont	Niu, 1997; Dong *et al.*, 2008
Brooksella canyonensis	0.9	Nankoweap Formation	Grand Ganyon. Arizona	jellyfish	Mudroll aggregate	Fedonkin & Runnegar, 1991
Protadelaidea howchini	0.9	Stonyfell Quartzite	Tea Tree Gully, South Australia	Giant arthropod	Mud flakes	David & Tillyard, 1936; Branagan, 2005
Medusoid	0.9	Nimbahera Shale	Madhya Pradesh, India	Vendobiont	Vendobiont	Runnegar, 1991
Metazoan burrow	1.0	Mixed Formation	Mindola North Pit, Zambia	Metazoan burrow	Cretaceous (?) termite burrow	Clemmy, 1978; Cloud *et al.*, 1980
Metazoan grazing traces	1.25	Allamore Formation	Millican Hills, Texas	Metazoan grazing trails	Wrinkled microbial mat	Breyer *et al.*, 1995
Flexuous annelid burrows	1.3	lower Siyeh Formation	Dawson Pass, Montana	Metazoan burrows	Shrinkage crack fills	Fenton & Fenton, 1937; Hofmann, 1991a
Planolites superbus, P. corrugatus	1.3	Greyson Shale	Niehart, Montana	Metazoan burrows	Deformed sandy lens	Hofmann, 1991a
Horodyskia moniliformis	1.5	Apekunny Formation	Glacier National Park, Montana	Eukaryote	Archaeo–sporalean	Retallack *et al.*, 2013a
Horodyskia sp. indet.	1.5	Manganese Group	Bangemall, W. Australia	Eukaryote	Archaeo–sporalean	Fedonkin *et al.*, 2008
Discoid radially furrowed impression	1.6	Pandwa Fall Sandstone	below Gangau Dam, India	Vendobiont	Vendobiont	Williams & Schmidt, 2003
burrows	1.6	Chorhat Sandstone	Chorhat Village, India	Metazoan burrows	Slime mold trail	Seilacher *et al.*, 1998; Seilacher, 2007
Ruyangichnus luoyensis	1.7	Beidajian Formation	Ruyang, China	Metazoan burrows	Colonial alga	Yang & Zhou, 1995
Torrowangea rosei	1.7	Beidajian Formation	Ruyang, China	Metazoan burrows	Slime mold trail	Yang & Zhou, 1995
Vermiform trace fossils	1.7	Baicaoping Formation	Lushan, China	Metazoan burrows	Slime mold trail	Hu *et al.*, 1997
Medusichnites sp. indet.	1.8	Animikie Group	Thunder Bay, Canada	Jellyfish	Mud–drag marks	Hofmann, 1971
Cyclomedusa sp. indet.	1.9	Stirling Range Form.	Stirling Range, W. Australia	Vendobiont	Microbial colony	Bengtson *et al.*, 2007
Myxomitodes stirlingensis	1.9	Stirling Range Form.	Stirling Range, W. Australia	Multicellular organism trails	Slime mold trail	Bengtson *et al.*, 2007; Bengtson & Rasmussen, 2009
cf. *Skolithos* sp. indet.	2.0	Espanola Formation	Quirke Lake Ontario, Canada	Dewatering structures	Dewatering structures	Hofmann, 1991a
cf. *Skolithos* sp. indet.	2.0	Akaitcho Formation	Reliance, NWT, Canada	Metazoan trace fossils	Dewatering structures	Hofmann, 1971, 1991a
Gabonionta	2.1	FB2 Formation	Franceville, Gabon	Large colonial organisms	Microbial colony	El Albani *et al.*, 2010, 2016

Diskagma buttoni	2.2	Hekpoort Basalt	Waterval Onder, South Africa	Archaeo–sporalean	Archaeo–sporalean	Retallack *et al.*, 2013b
Kempia huronense	2.2	Mississagi Quartzite	Near Espanola, Canada	Colonial organism	Microbial colony	Hofmann, 1971
Kempia huronense	2.3	Gowganda Formation	Sudbury and Iron Bridge, Canada	Colonial organism	Microbial colony	Hofmann, 1971
Metazoan burrows	2.3	Ajibik Quartzite	Ishpeming, Michigan	Metazoan burrows	Cyanobact–erial ropes	Faul, 1949, 1950, Hoffman, 1991a
Rhysonetron byei	2.3	Lorraine Formation	Desbarats, Ontario, Canada	Vendobiont	Rolled mud flakes	Hofmann, 1971, 1991a
Rhysonetron lahti	2.3	Bar River Formation	Flack Lake, Ontario, Canada	Vendobiont	Rolled mud flakes	Hofmann, 1971, 1991a
Tubular structures	2.5	Sugarloaf Quartzite	Medicine Bow Pk, Wyoming	Soil microbes	Cyanobact–erial ropes	herein
Sediment–filled tubular dubiofossils	2.5	Medicine Pk Quartzite	Medicine Bow Pk, Wyoming	Metazoan trace fossils	Cyanobact–erial ropes	Kauffman & Steidtmann, 1981

(Allwood *et al.*, 2006, 2007), other microbialites (Rasmussen *et al.,* 2009), carbonaceous compressions (Hoffman, 1991b; Dong *et al.,* 2008), or biomarkers (Neuweiler *et al.*, 2009; Planavsky *et al.*, 2009; Gold, 2018). Most postulated pre–Ediacaran megascopic sandstone trace fossils have been relegated to dubiofossils or pseudofossils (Faul, 1949, 1950; David & Tillyard, 1936; Häntzschel, 1975; Clemmy, 1978; Cloud *et al.*, 1980; Hoffman, 1971, 1991a). Other pre–Ediacaran sandstone megafossils are comparable with Ediacaran quilted fossils (vendobionts) and discoids, which themselves are problematic (Runnegar, 1991; Runnegar & Fedonkin, 1991; Narbonne *et al.,* 1994; Yang & Zhou, 1995; Hu, 1997; Niu, 1997; Williams & Schmidt, 2003; Zhang *et al.*, 2006; Fedonkin *et al.*, 2008; Dong *et al.*, 2008; El Albani *et al.,* 2010; Meert *et al.*, 2011; Retallack *et al.*, 2013a–b).

Despite skepticism, discoveries of megafossils continue to revive hope for pre–Ediacaran metazoans. Possible worm like trails of *Myxomitodes stirlingensis* (Bengtson *et al.*, 2007) from the Stirling Range Formation of Western Australia, dated between 2000 Ma and 1800 Ma (Rasmussen & Muhling, 2007), may have been rolling trails of giant shelled–amoebae, comparable with living marine *Gromia sphaerica* (Matz *et al.*, 2008; Bengtson & Rasmussen, 2009), or trails of the slug–phase of slime molds (Retallack, 2013; Retallack & Mao, 2019). Putative burrows in the Chorhat Sandstone near Chorhat Village, India (Seilacher *et al.*, 1998), dated between 1628 ± 8 and 1599 ± 8 Ma (Ray *et al.*, 2002; Rasmussen *et al.*, 2002), could be artefacts of gas bubbles (Seilacher, 2007), but also are similar to slime mold trails (Retallack & Mao, 2019). Other possible slime mold trails have been recorded from the 1700 Ma Baicaoping and Beidajian Formations of the Ruyang Group in western Henan, China (Yang & Zhou, 1995; Hu, 1997). Radially quilted "Gabonionta", 15–36 mm long, permineralized by pyrite between laminae of grey shales of the FB Formation near Franceville, Gabon, are dated between 2099 ± 30 Ma and 2083 ± 30 Ma, and described as "large colonial organisms with coordinated growth" (El Albani *et al.*, 2010, 2019). Although structurally comparable with cellular slime molds such as *Dictyostelium* (Bonner, 2009), Vendobionta such as *Rutgersella* (Retallack, 2015a), and bacterial colonies (Ben–Jacob *et al.*, 1994; Shapiro, 1998), these may have been Archaeosporalean fungi like *Horodyskia* (Retallack *et al.*, 2013a) and *Diskagma* (Retallack *et al.*, 2013b).

Less easy to dismiss as non–metazoan are putative burrows from the Palaeoproterozoic (2.3 Ga) Medicine Peak Quartzite of Wyoming, because these structures are deep within sedimentary beds (Kauffman & Steidtmann, 1981), unlike surficial bubble artefacts (Seilacher, 2007), rolling trails (Bengtson & Rasmussen, 2009) or spreading microbial colonies (Ben–Jacob *et al.*, 1994; Shapiro, 1998). A number of arguments that these tubular structures were fossils, rather than pseudofossils or dubiofossils, were advanced by Kauffman & Steidtmann (1981): (1) tubular structures are truncated by overlying beds, thus synsedimentary; (2) tubular structures are filled with sediment from above, thus synsedimentary; (3) tubular structures modify pre–existing bedding and decline in abundance downward from truncated surfaces, thus postdepositional; (4) tubular structures branch with random orientation both vertically and horizontally, thus neither current markings nor metamorphic lineation; (5) tubular structures have a log–normal distribution of diameters, as in organisms of indeterminate growth, unlike normal distribution of determinate organisms and of nodules, concretions and sand volcanoes; (6) tubular structures are most common in a particular sedimentary facies (interpreted by them as intertidal to subtidal); (7) tubular structures form a variety of recognizable forms which resemble Phanerozoic fossils (especially trace fossils). While parts of these arguments are questioned here (in parentheses above), these observations are compelling evidence that these are genuine fossils.

Additional tubular fabrics from the same area of Wyoming are described here. The new specimens share all seven features outlined above for Medicine Peak Quartzite

fossils, but come from red beds in an outcrop of Sugarloaf Quartzite, a stratigraphically higher and geologically younger rock unit than the Medicine Peak Quartzite, dated to *ca*.2200 Ma (Houston *et al.*, 1992; Kauffman *et al.*, 2009). The newly discovered tubular features are abundant, well exposed, little weathered, and appear to have grown in place within palaeosols. The possibility of a palaeosol context for some of these fossils raises the following important questions not considered by Kauffman & Steidtmann (1981), or previous studies of megafossils in Palaeoproterozoic quartzites (Seilacher, 2007; Bengtson *et al.*, 2007). Were they body fossils rather than trace fossils? Did the fossils live in soil rather than under the sea? A better modern analog for these fossils may be the varied cyanobacterial, fungal and other megascopic consortia of microbes in modern soils of extreme environments, such as microbial earths (Retallack, 1992, 2012a), palaeodesert microbial mats (Simpson *et al.*, 2013) or supratidal mats (Homann *et al.,* 2015).

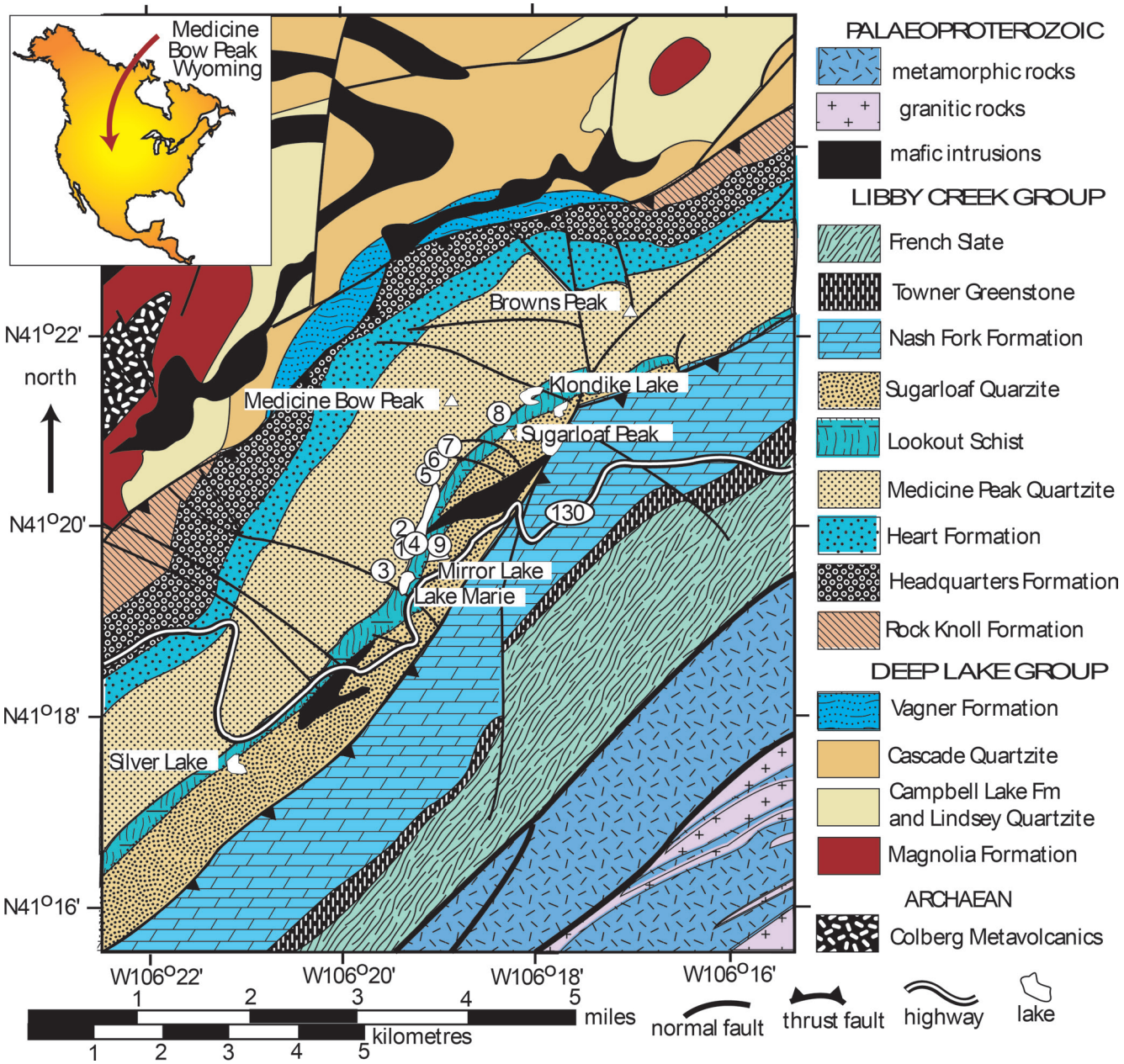

Fig. 1—Localities near Medicine Bow Peak, Wyoming. Localities 1–8 in scree from cliffs of the upper Medicine Peak Quartzite were collected by Kauffman & Steidtmann (1981): fossils from an outcrop of Sugarloaf Quartzite at locality 9 are reported here.

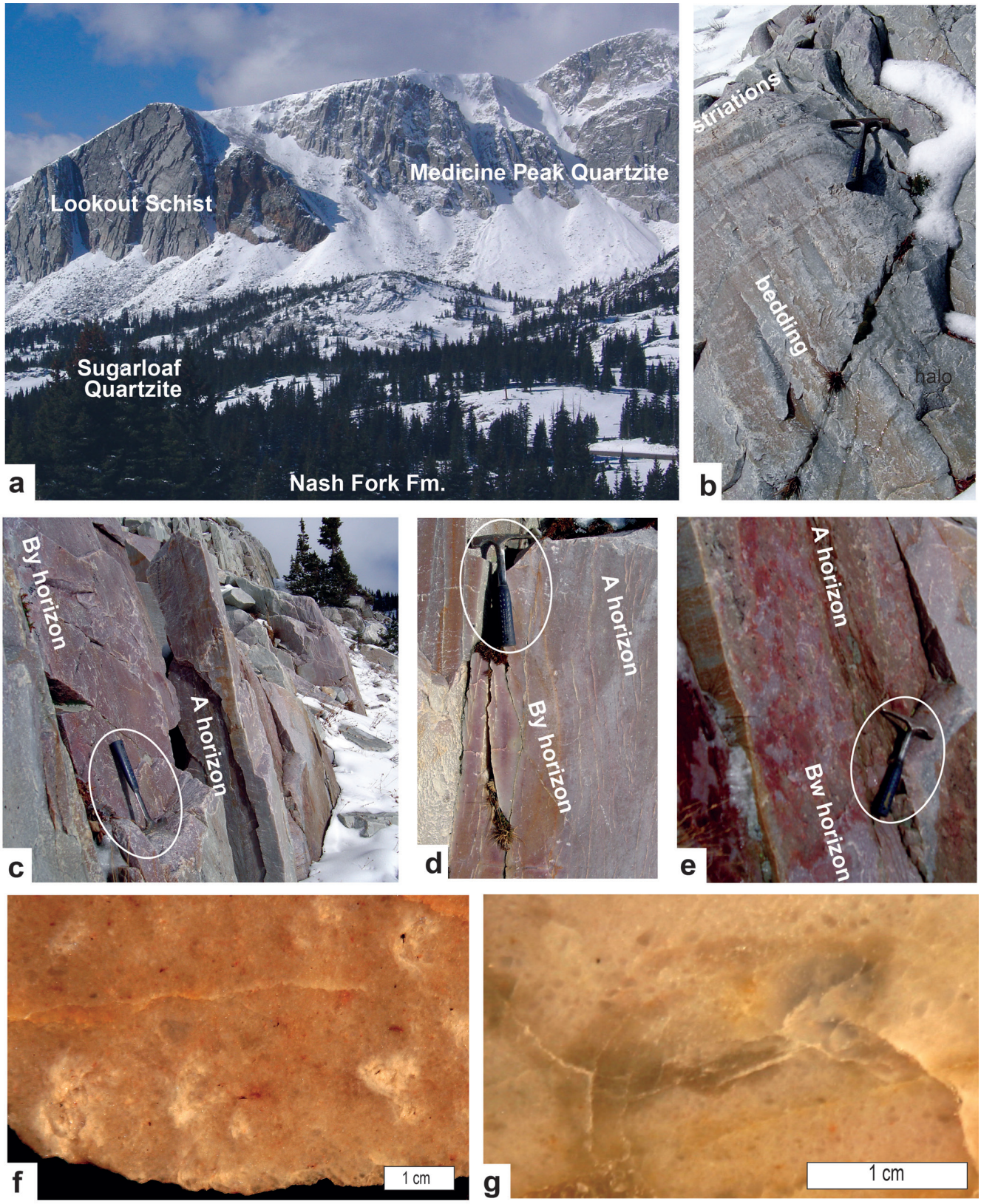

Fig. 2—Field photographs of palaeosols and localities in the 2 Ga Sugarloaf Quarzite near Medicine Bow Peak, Wyoming: (A), overview of snow–covered scree of Medicine Peak Quartzite and *roche moutonée* of Sugarloaf Quarzite locality 9 (right of label): (B), glacially striated outcrop of Sugarloaf Quartzite at locality 9 indicating that it is not a displaced block: (C–D), quartz–haloed gypsum pseudomorphs: (E–F), Mirror palaeosols at locality 9 (4.2 and 15 m in Fig.3): (G), Medicine palaeosol at locality 9 (13 m in Fig. 3). Hammers for scale (length 25 cm) indicated by white ellipses.

GEOLOGICAL SETTING

The Medicine Peak and Sugarloaf Quartzites are part of a thick succession of fluvial, intertidal and shallow marine sandstones, shales and stromatolitic limestones exposed in glacial valleys at the crest of the Medicine Bow Range, 62 km west of Laramie, Wyoming (Karlstrom *et al.,* 1983; Houston *et al.*, 1992; Chamberlain, 1998). The Medicine Peak Quartzite forms steep walls of glacial cirques, but the Sugarloaf Quartzite sampled near Mirror Lake is a low ridge with prominent glacial striations (locality 9 in Fig. 1; low cliffs of Fig. 2A, E). Oscillation ripples in this outcrop (Fig. 2B, E) serve as geopetal structures, indicating a dip of 76° east and a strike of magnetic azimuth 202°, coherent with local strike of overlying and underlying beds. This is a large outcrop (200 m long and 20 m thick) surrounded by boulder till, and with glacial striations (Fig. 2B). Because this striation is in the direction of local glacial advance, this outcrop is not a displaced morainal boulder, but a *roche moutonnée* of underlying bedrock (Fig. 1).

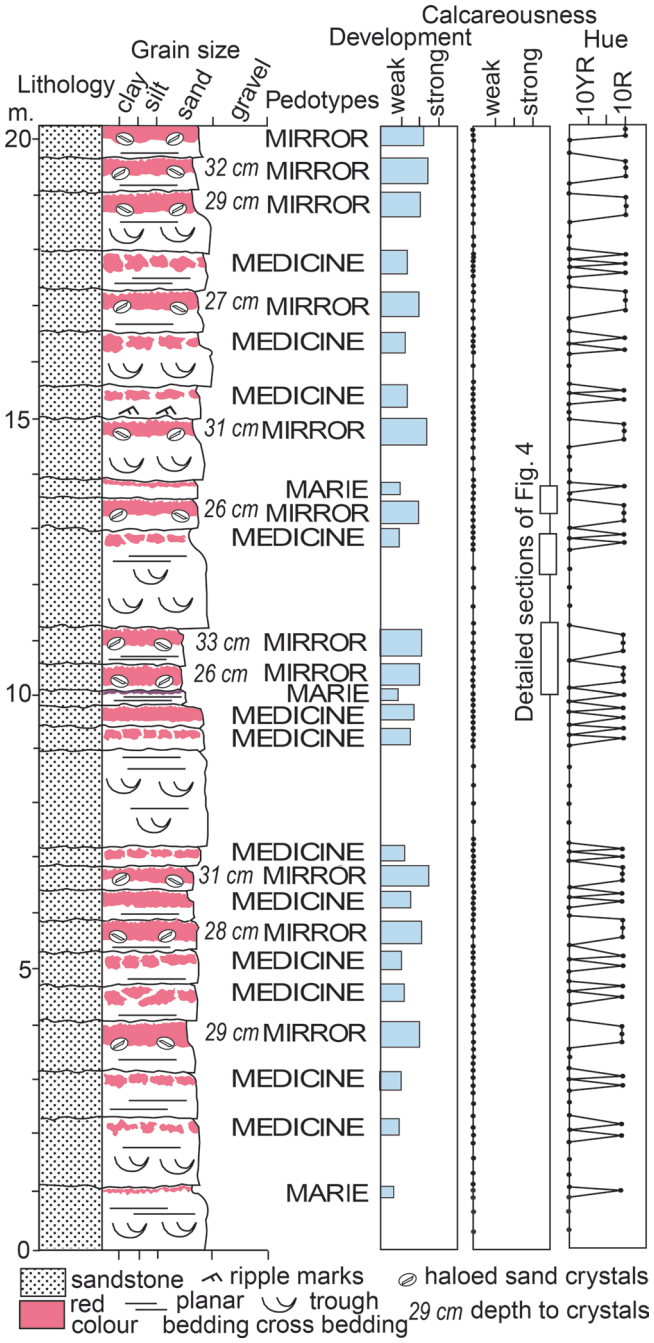

Fig. 3—Measured section of Palaeoproterozoic palaeosols in Sugarloaf Quartzite at locality 9 east of Mirror Lake, near Medicine Bow, Wyoming. Development and calcareousness is based on a scale of Retallack (1997) and hue measured from a Munsell chart.

Both Medicine Peak and Sugarloaf Quartzites are intruded by, so older than Gaps Intrusions dated by Rb–Sr at 2000–2150 Ma. They are younger than detrital zircons from the Magnolia Formation dated using U–Pb at 2451 ± 12 Ma, and are older than metagabbro intruding the Cascade Quartzite dated by U–Pb in zircon at 2092 ± 4 Ma (Houston *et al.*, 1992). Medicine Peak Quartzite is dated at *ca*. 2,300 Ma based on detrital zircons mostly within the age range 2600–2700 Ma (Sawada *et al.*, 2018). Both Medicine Peak and Sugarloaf Quartzites have strongly sutured quartz grains, fuchsite and sericite, due to regional greenschist facies metamorphism. This metamorphism is dated within the intervening Lookout Schist (Fig. 1) by Rb–Sr using whole rock at 1680 ± 60 Ma (Houston *et al.*, 1992), and regionally at 1,780–1,750 Ma (Jones *et al.*, 2010). Sugarloaf Quartzite is thus *ca*. 2,200 Ma in age.

Prior to this metamorphism the Medicine Peak and Sugarloaf Quartzites accumulated within a rift valley (Karlstrom *et al.*, 1983). The intervening Lookout Schist with thin dolostones and banded iron formations, and the overlying Nash Fork Formation with stromatolitic dolostones, have both been interpreted as shallow marine (Karlstrom *et al.*, 1983; Bekker *et al.*, 2003). However, the Medicine Peak and Sugarloaf Quartzites include conglomeratic bands, trough cross bedding, ripple marks and flaggy bedding interpreted as deposits of rivers and coastal deltas (Kauffman & Steidtmann, 1981; Karlstrom *et al.*, 1983). Palaeocurrent data from planar and trough cross–bedding within both quartzites provide evidence of flow to the southwest, where the fault–bounded valley opened up to the ocean (Karlstrom *et al.*, 1983). This valley was on the margin of greater Laurentia ("Atlantica"), then part of a larger continent of Protopangea, and at a palaeolatitude of 43 ± 8° (Piper, 2010).

MATERIALS AND METHODS

Fieldwork during November 2007, failed to collect more of the intriguing fossils reported by Kauffman & Steidtmann (1981) because of deep snow, but led to new fossil discoveries in outcrops of Sugarloaf Quartzite, close to state highway 130 and Mirror Lake campground. The exposed section

Table 2—Chemical analyses (wt %) of palaeosols in Sugarloaf Quartzite, Wyoming.

Sample	SiO_2	TiO_2	Al_2O_3	FeO	Fe_2O_3	CaO	MgO	Na_2O	K_2O	Cr_2O_3	MnO	P_2O_5	SrO	BaO	LOI	Total
R3448	97.01	0.07	0.46	0.39	0.4	0.03	0.14	0.01	0.14	0.04	<0.01	0.011	0.009	0.01	0.1	98.41
R3449	98.01	0.07	0.6	0.38	0.38	0.03	0.03	0.01	0.17	0.04	<0.01	0.016	0.009	0.01	0.09	99.45
R3450	97.21	0.06	0.34	0.32	0.28	0.009	0.04	0.009	0.11	0.02	<0.01	0.01	0.009	0.01	0.06	98.15
R3451	97.75	0.07	0.27	0.38	0.4	0.01	0.01	0.009	0.09	0.04	<0.01	0.014	0.009	0.01	0.03	98.7
R3452	98.31	0.08	0.35	0.26	0.35	0.009	0.03	0.009	0.11	0.04	<0.01	0.012	0.009	0.01	0.05	99.34
R3453	97.96	0.05	0.27	0.38	0.42	0.009	0.01	0.009	0.09	0.05	<0.01	0.008	0.009	0.01	–0.03	98.83
R3454	97.61	0.06	0.32	0.38	0.33	0.009	0.02	0.009	0.1	0.04	<0.01	<0.001	0.01	0.009	0.04	98.53
R3455	97.89	0.05	0.29	0.26	0.26	0.009	0.01	0.009	0.1	0.03	<0.01	0.01	0.009	0.01	0.05	98.7
R3456	97.75	0.06	0.28	0.32	0.32	0.009	0.02	0.01	0.08	0.03	<0.01	0.01	0.009	0.01	0.07	98.64
R3457	98.34	0.05	0.24	0.19	0.23	0.009	0.01	0.009	0.08	0.03	<0.01	<0.001	0.01	0.009	0.06	99.05
R3458	97.7	0.07	0.26	0.26	0.28	0.009	0.01	0.009	0.09	0.03	<0.01	<0.001	0.009	0.009	0.05	98.5
R3460	98.15	0.04	0.29	0.39	0.43	0.009	0.02	0.009	0.08	0.03	<0.01	<0.001	0.01	0.009	0.04	99.09
R3461	97.55	0.04	0.26	0.26	0.45	0.009	0.01	0.009	0.06	0.02	<0.01	<0.001	0.009	0.009	0.06	98.45
R3462	97.6	0.04	0.24	0.19	0.44	0.009	0.01	0.009	0.05	0.03	<0.01	<0.001	0.009	0.009	0.06	98.47
R3463	98.32	0.05	0.37	0.32	0.29	0.009	0.01	0.009	0.12	0.03	<0.01	0.008	0.009	0.01	0.02	99.23
Error	2.705	0.06	0.83		0.395	0.22	0.18	0.11	0.13		0.025	0.035			0.35	

Note: Analyses are by XRF with Pratt titration for FeO. Errors are from 10 replicate analyses of the standard, CANMET SDMS2 (British Columbia granodioritic sand).

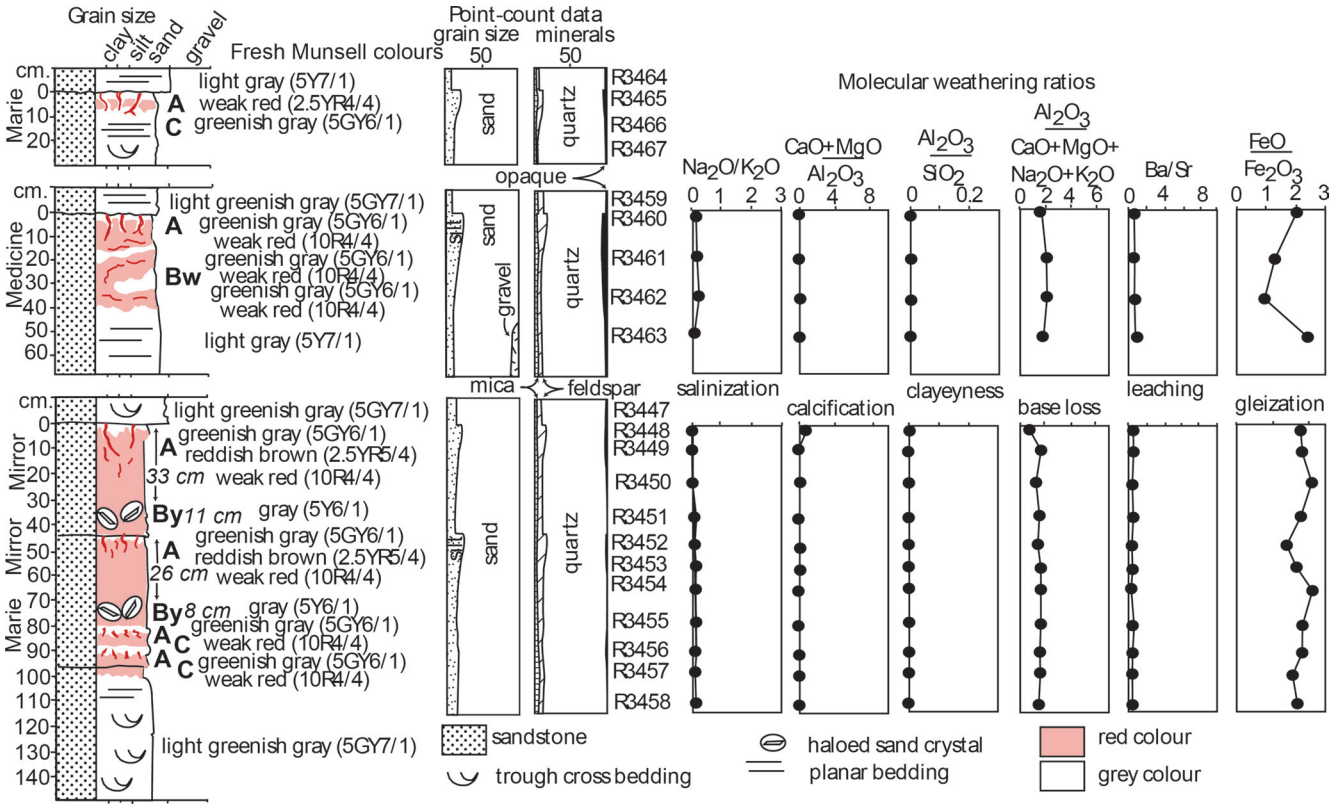

Fig. 4—Chemical and petrographic data on Palaeoproterozoic palaeosols in the Sugarloaf Quartzite at Mirror Lake, Wyoming, at stratigraphic levels indicated in Fig. 3. Mineral and grain size proportions are from point counting petrographic thin sections (Table 2). Molecular weathering ratios are designed to reflect particular weathering processes, and are based on XRF chemical analyses (Table 3). Sample numbers (prefix R–) are archived in the Museum of Natural and Cultural History, University of Oregon.

immediately west of Mirror Lake (N41.33984° W106.31979°) was measured with cloth tape (Fig. 3) and representative specimens were collected of beds with tubular structures (Fig. 4). The percentage of gypsum pseudomorphs in individual beds was estimated in the field using a comparative chart (Terry & Chilingar, 1955).

Selected samples were analyzed for major elements by XRF with Pratt titration for FeO, using CANMET SDMS2 standard (British Columbia granodioritic sand) by ALS Chemex of Vancouver, British Columbia, Canada (Table 2). Petrographic thin sections revealed microscopic details of the fossils, and were point–counted using a Swift automated counter for percent grain size, using an eyepiece micrometer, and for mineral content under crossed nicols (Table 3). Chemical analyses using the Cameca S x100 electron microprobe by J.J. Donovan in the Center for Advanced Materials Characterization of Oregon (CAMCOR) at the University of Oregon focused on a transect of 132 analyses across a polished thin section of a sand crystal in specimen R3457.

All specimens described here are housed in the Condon Collection, Museum of Natural and Cultural History, University of Oregon, Eugene (specimens F115605–15617, F116171–16176, R3447–R3467). Tubular structures and comparative modern material were measured using Vernier calipers (Table 4). Resulting size distributions were tested for normality by Kolmogorov's D and Shapiro–Wilk's W using the computer program JMP (Table 5). Comparable specimens described by Kauffman & Steidtmann (1981) were examined in the Department of Paleobiology, Smithsonian Institution, Washington DC, and in the collections of the Department of Geological Sciences, Indiana University, Bloomington. Indiana material was uncatalogued during 2016 inspection, and only two specimens and thin sections remained at the Smithsonian for examination (USNM 243015, 243016).

Modern comparative material examined includes microbial earths observed June 26, 2007, at Lake Mungo, New South Wales, Australia (S33.73497° E145.05594°), and the lichen *Cladonia phyllophora* collected June 7, 2008, from Fishtrap Lake, Montana (N47.864430° W115.197730°). Slime molds (*Lycogala epidendrum*) and puffballs (*Morganella pyriformis*) illustrated for comparison were photographed at the Cascade Mycological Society annual Mount Pisgah Mushroom Show October 25, 2009, and are from Hendricks Park, Eugene, Oregon (N44.037376° W123.057456°).

PALAEOPROTEROZOIC PALAEOSOLS

Description

Quartz sandstones of the Sugarloaf Quartzite are thick–bedded, and massive, with few recognizable sedimentary

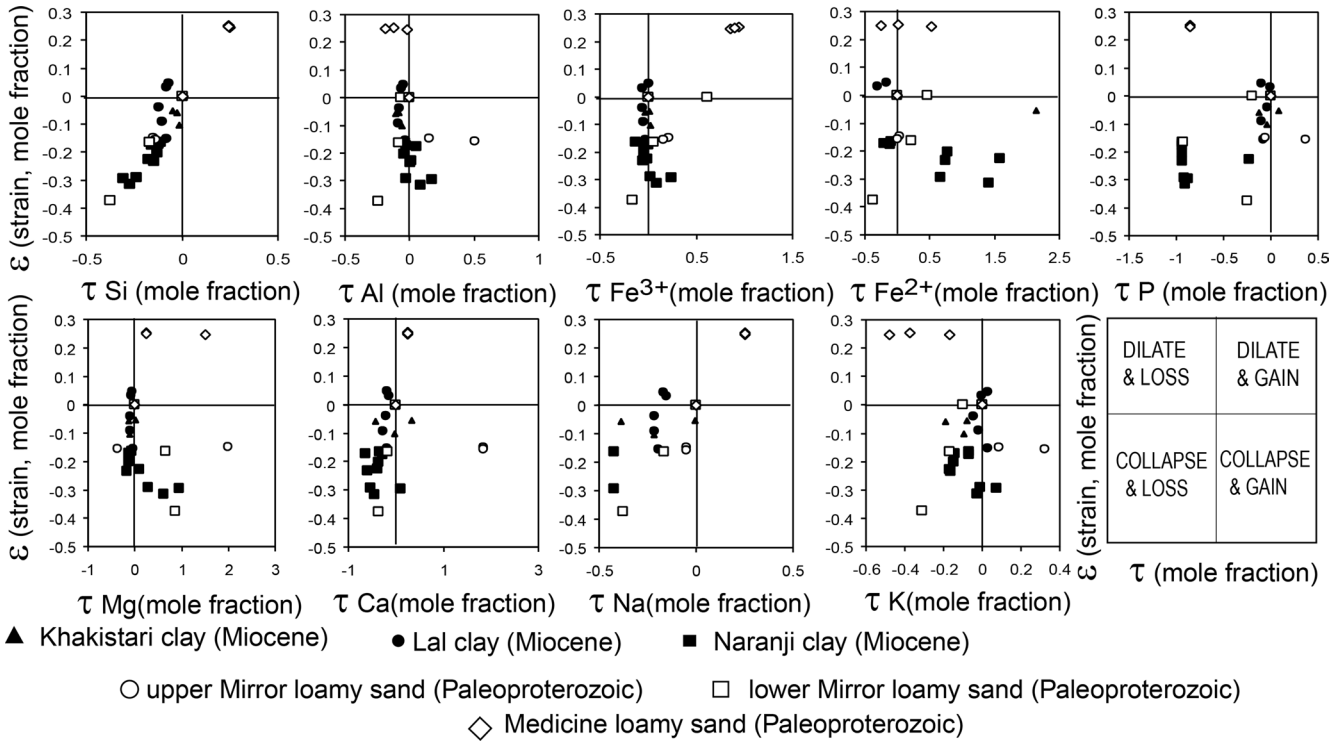

Fig. 5—Mass balance geochemistry of Medicine and Mirror palaeosols, including estimates of strain from changes in an element assumed stable (Ti) and elemental mass transfer with respect to an element assumed stable (Ti following Brimhall *et al.*, 1992), and by comparison with Miocene palaeosols from Pakistan, also formed in quartzofeldspathic alluvium (Retallack, 1991). Zero strain and mass transfer is the parent material lower in the profile: higher horizons deviate from that point due to pedogenesis.

Table 3—Minerals and grain size (vol.%) of palaeosols in Sugarloaf Quartzite, Wyoming.

Sample	Quartz	Feldspar	Opaque	Mica	Rock fragments	Silt	Sand	Gravel
R3447	89.2	2.6	0.6	6.8	0.8	13.2	86.8	0
R3448	87.0	2.8	0	9.6	0.6	17.6	824	0
R3449	88.0	2.0	1.4	7.8	0.8	11.0	89.0	0
R3450	90.2	3.0	0.8	5.6	0.4	8.6	91.4	0
R3451	92.8	1.8	0.4	4.8	0.2	12.8	87.2	0
R3452	89.6	0.8	0.4	9.2	0	18.4	81.6	0
R3453	91.4	1.2	1.6	5.2	0.6	12.6	87.4	0
R3454	90.6	2.6	0.4	4.8	1.6	10.2	89.8	0
R3455	92.0	2.2	0.6	4.4	0.8	8.2	91.8	0
R3456	91.8	2.2	1.2	4.4	0.4	14.4	85.6	0
R3457	90.2	5.0	1.8	2.8	0.2	10.4	89.6	0
R3458	92.2	3.2	0.6	3.6	0.4	12.4	87.6	0
R3459	86.2	4.2	1.6	7.8	0.2	9.8	90.2	0
R3460	87.4	1.4	2.6	6.0	2.6	19.6	80.4	0
R3461	86.0	3.6	4.4	4.8	1.2	13.8	86.2	0
R3462	89.2	2.4	4.8	2.2	1.4	11.4	88.6	0
R3463	90.4	3.0	0.8	4.6	1.2	12.6	74.4	13.0
R3464	93.2	3.4	0.6	1.8	1.0	10.6	89.4	0
R3465	88.2	4.2	1.0	4.8	1.8	23.2	76.8	0
R3466	90.4	4.4	1.2	3.8	0.2	13.0	87.0	0
R3467	91.0	3.0	1.4	2.8	1.8	12.6	87.4	0

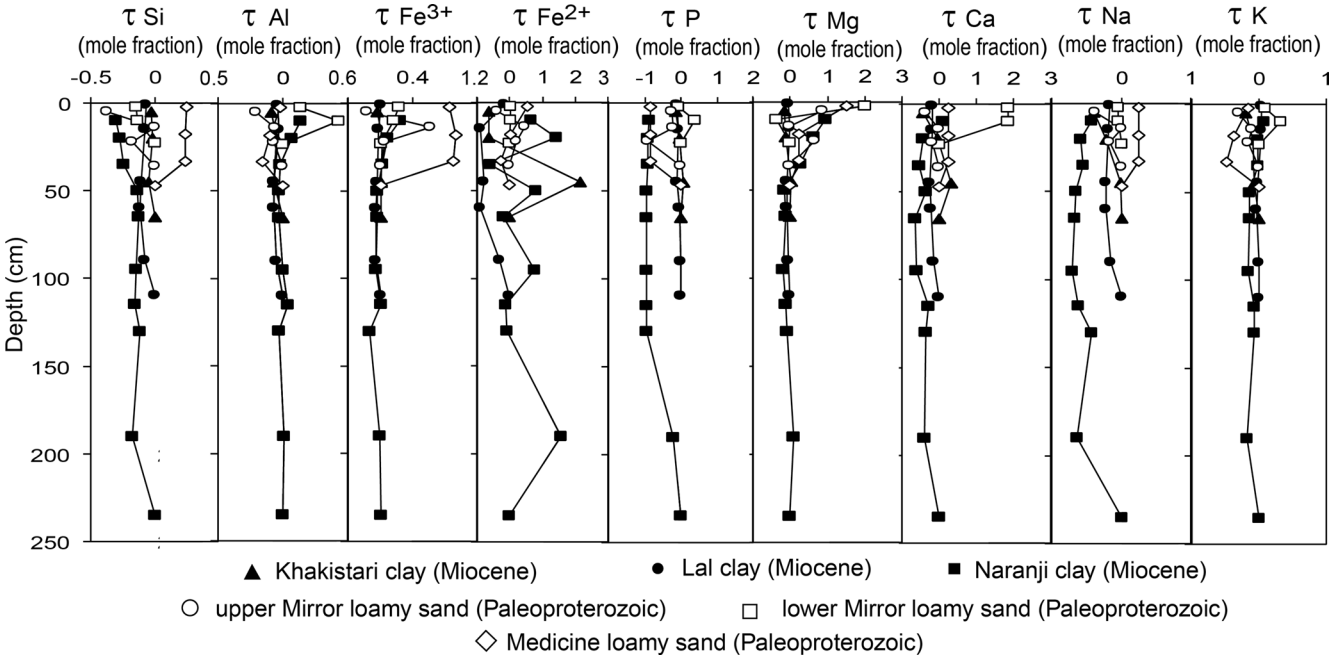

Fig. 6—Mass transfer with depth of Medicine and Mirror palaeosols and some Miocene palaeosols from Pakistan (Retallack, 1991).

Table 4—Measured diameters of tubular structures in Sugarloaf Quartzite (mm).

Specimen	Kind of fossil	Palaeosol	Mean ± standard deviation	Median	Mode	Range	Number of measurements
F115611	Slender tubes	Marie	0.8 ± 0.3	0.8	0.6	0.2–2.9	600
F116174	Slender tubes	Mirror	0.8 ± 0.3	0.7	0.6	0.2–2.3	124
F116175	Slender tubes	Mirror	0.7 ± 0.3	0.6	0.4	0.2–1.4	113
F116173	Slender tubes	Medicine	0.8 ± 0.3	0.8	0.7	0.2–1.4	120
F116176	Slender tubes	Marie	0.5 ± 0.2	0.5	0.5	0.2–1.1	115
F116172	Slender tubes	Marie	0.5 ± 0.2	0.4	0.4	0.2–1.1	113
F115617	Stout tubes	Marie	1.9 ± 0.5	1.9	1.5	0.8–3.3	123
F115606	Stout tubes	Marie	2.2 ± 1.0	2.1	1.1	0.6–5.0	43
F156114	Thick tube with bulb	Marie	4.7 ± 0.6	4.7	4.7	3.8–5.9	15

structures (Fig. 2E–F). Some ripple marks, planar bedding and trough–cross bedding were seen (Figs 3–4). These sedimentary structures have been variably destroyed by homogenization and reddening with hematite. The boundary between the red and homogeneous upper part of the bed and the grey lower part of the bed is gradational, but the uppermost contacts of the homogeneous part of the bed are sharply truncated.

Some beds also contain distinctive crystal pseudomorphs (Fig. 2F–G), in diffuse, strata–concordant, horizons near the zone of transition between the red homogeneous upper part of the bed and the grey lower part of the bed with ripple marks, trough cross bedding and planar bedding. These grey crystals have sharp interfacial angles, comparable with gypsum crystals, but also have a rounded white halo. Thin sections demonstrate that neither the crystal pseudomorph, nor its enveloping halo are salts now: both are silica–cemented sandstone. The size of these haloed pseudomorphs varies from 5 to 20 mm, and the largest ones are found in the thickest, reddest and most homogenized beds.

Grain size and mineral composition of these palaeosols from point counting of thin sections shows an abrupt change from overlying quartz–rich sediments to silty and feldspathic surface horizons. These surface horizons grade downward into sandier quartz–rich subsurface horizons (Fig. 4; Table 2). These rocks are all quartz–dominated.

Chemical analysis of selected beds for major elements by XRF reveals slight surficial base depletion and striking surficial iron oxidation within each bed (Table 3). Quartz dominance of minerals is reflected also in very low levels of alkalies, alkaline earths and alumina in these rocks, and little change with depth. Electron microprobe traverses across polished sections of crystal pseudomorphs revealed traces of Ba (0.0048 ± 0.01 wt %, maximum 0.022 wt %), Ca (0.012 ± 0.81 wt %, maximum 6.54 wt %), Na (0.0025 ± 0.023 wt%, maximum 0.18 wt %), Mg (0.0017 ± 0.016 wt %, maximum 0.12 wt %), and K (0.064 ± 0.41 wt %, maximum 3.34 wt %), confirming XRF analyses. The pseudomorphs may have been sand crystals of gypsum ($CaSO_4.2H_2O$).

A more detailed accounting of geochemical change within beds following Brimhall *et al.* (1992) is mass transfer of elements in a soil at a given horizon ($\tau_{j,w}$ in mole fraction) calculated from the bulk density of the soil (ρ_w in g.cm^{-3}) and parent material (ρ_p in g.cm^{-3}) and from the chemical concentration of the element in soils ($C_{j,w}$ in weight %) and parent material ($C_{j,p}$ in weight %). Changes in volume of soil during weathering are called strain by Brimhall *et al.* (1992), and estimated from an immobile element in soil (such as Ti used here) compared with parent material ($\varepsilon_{i,w}$ as a mass fraction). The relevant equations 1 and 2 (below) are the basis for calculating divergence from parent material composition due to soil formation.

$$\tau_{j,w} = \left[\frac{\rho_w \cdot C_{j,w}}{\rho_p \cdot C_{j,p}}\right]\left[\varepsilon_{i,w} + 1\right] - 1 \quad \text{— equation 1}$$

$$\varepsilon_{i,w} = \left[\frac{\rho_p \cdot C_{j,p}}{\rho_w \cdot C_{j,w}}\right] - 1 \quad \text{— equation 2}$$

These calculations were performed for three beds of the Sugarloaf Quartzite, assuming a parent material comparable with the lower parts of the individual beds. Most of the beds fall within arrays of the collapse and loss, but one bed (Medicine of Figs 5–6) falls into the field of dilate and gain. There are slight gains in Mg and Ca in some beds with crystal pseudomorphs (Mirror of Figs 5–6)

Interpretation

These various field, petrographic and geochemical observations are evidence that the Sugarloaf Quartzite is a succession of palaeosols with different degrees of development of a surface (A) horizon, and gypsum sand crystals in a subsurface (By) horizon (Figs. 3–4). These crystal casts are now quartz grains cemented by quartz, and have euhedral outline comparable with laths and fishtail twins of gypsum (Retallack, 1983), as well as white nodularized

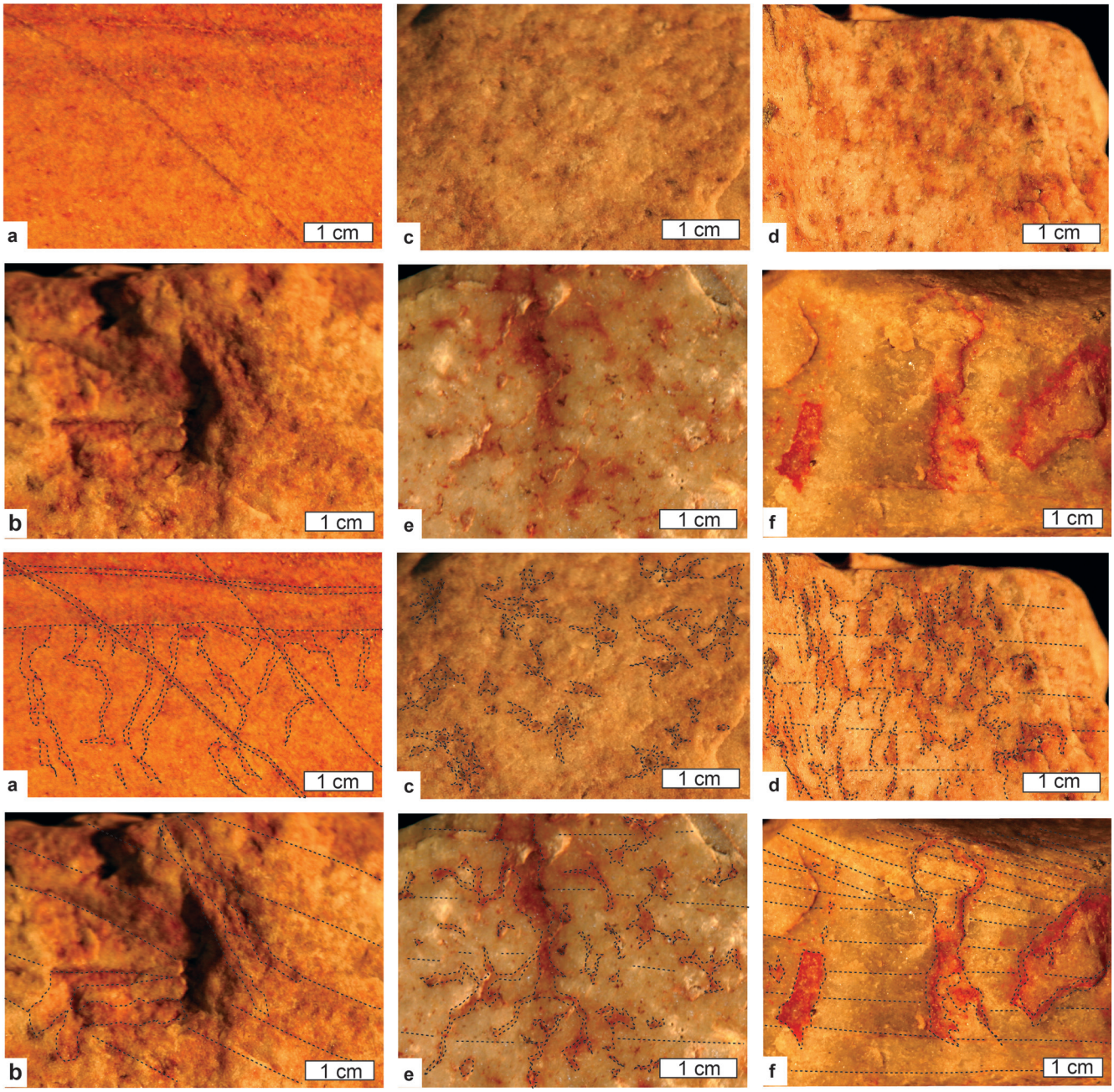

Fig. 7—Palaeoproterozoic problematic megafossils, with and without outlined fossil margins and bedding planes: (a–b, e) stout tubes: (c–d), slender ramifying tubes: (f), thick tubes with globules in hand specimens horizontal (c) and vertical to bedding (a–b, d–f). Specimen numbers in the Condon Collection, Museum of Natural and Cultural History, University of Oregon are (a) F115617, (b) F115611, (c–d) F115611, (e) F115606, (f) F115614.

alteration haloes (Fig. 2D). These are comparable with sand crystals formed by precipitation of gypsum around quartz grains of largely dry matrix unique to moderately developed soils and palaeosols (Retallack & Kirby, 2007; Retallack, 2008). In contrast, evaporitic sedimentary sulfates have clean crystals within laminae displacing matrix or forming thick evaporite beds (Ziegenbalg *et al.*, 2010). Both the reddening and nodules have diffuse contacts with adjacent layers as is typical of palaeosols, in contrast to the abrupt sedimentary truncation of tops of the palaeosols (Fig. 2E–G).

Chemical analysis shows that these palaeosols are deeply weathered of alumina and bases overall (Fig. 4), and have also lost alumina and bases within individual beds (Mirror of Figs 5–6). Enrichment of titanium toward the top of the beds due its resistance to chemical weathering is characteristic of weathering (Brimhall *et al.*, 1992), whereas titanium present in heavy minerals such as ilmenite is concentrated at the base

Table 5—Tests for normality of size distributions by Shapiro–Wilk (W) and Kolmogorov (D) tests.

Specimen	Kind of fossil or modern	W	P of normal	D	P of log–normal	Conclusions
F115611	Slender tubes	0.667	<0.0001	0.032	0.146	Log–normal
F116174	Slender tubes	0.907	<0.0001	0.060	>0.15	Log–normal
F116175	Slender tubes	0.954	0.007	0.08	0.075	Log–normal
F116173	Slender tubes	0.989	0.484	0.062	0.048	Normal
F116176	Slender tubes	0.921	<0.0001	0.062	>0.15	Log–normal
F116172	Slender tubes	0.953	0.0006	0.046	>0.15	Log–normal
F115614	Thick tube with bulb	0.970	0.860	0.128	>0.15	Normal
F115617	Stout tubes	0.980	0.079	0.041	>0.15	Normal
all	Slender tubes	0.778	<0.0001	0.039	<0.01	Log–normal
C393	*Cladonia phyllophora* podetia	0.964	<0.0001	0.026	>0.15	Log–normal
C393	*Cladonia phyllophora* apothecia	0.983	0.424	0.124	<0.01	Normal

of sedimentary beds. Sedimentation is the explanation for dilation and gain in most elements seen in one bed with clear relict bedding (Medicine of Figs 5–6), which was reversed with more substantial pedogenesis (Mirror of Figs 5–6). Weathering trends of collapse and loss in Mirror palaeosols are comparable with those of Miocene palaeosols from Pakistan plotted for comparison (Figs 5–6). Compared with these Miocene palaeosols of quartzofeldspathic sediments in semi–arid mid–latitude woodlands, Sugarloaf palaeosols show strong oxidation (Fe^{3+} enrichment), modest gleization (Fe^{2+} enrichment), and comparable base and phosphorous depletion, desilication, and alumina retention.

Three different kinds of Sugarloaf Quartzite palaeosols were recognized in the field (named pedotypes of Figs 2E–G, 3–4, Table 6). Bedding is only partly disrupted and weak red (2.5YR4/1) mottles sparse in the Marie pedotype, but little bedding and thick, weak red (10R4/4) subsurface horizons mark the Medicine pedotype (Figs 2E, 3,4). The Mirror pedotype has disrupted bedding for a thickness of 30–40 cm and a diffuse subsurface horizon of scattered sand crystals (Fig. 2C–D).

Burial alteration

Palaeosols are altered during burial in a variety of ways that need to be considered before proceeding with their palaeoenvironmental interpretation. Palaeosols of the Sugarloaf Quartzite were subjected to regional biotite–grade greenschist facies metamorphism at burial pressures of as much as 4 kbar, temperatures of 400°C and depths of 4.2 km (Chamberlain *et al.*, 1993; Chamberlain, 1998). The quartzite is extremely hard, splintering into dangerously sharp fragments under a sledge hammer. The quartzite was cemented by syntaxial rims of silica during deep burial. Its grain size has been coarsened by aggrading neomorphism during metamorphism to interlocking and sutured contacts (Fig. 8). Cementation and neomorphism are alterations that may have been accompanied by evaporite dissolution and replacement of the former gypsum in the palaeosols (Becker *et al.*, 2003), as in other Precambrian metamorphic terrains (Barley *et al.*, 1979; Nabhan *et al.*, 2016; Retallack *et al.*, 2016; Retallack, 2018). Metamorphism has converted clays to fuchsite and sericite (Crichton & Condie, 1993), but left feldspar and rock fragments intact (Table 3). There is no hint of potash metasomatism from very low potash values (Table 1). Nor did metamorphism proceed to the chemical reduction of hematite to magnetite (Thompson, 1972). Well preserved drab haloes and surfaces to some palaeosols (Fig. 3) are comparable with burial gleization of soils within decades of burial (Retallack, 1997).

Comparable palaeosols

Many palaeosols are known from Precambrian geological unconformities (Rye & Holland, 1998), but also from Precambrian sedimentary sequences. Most similar to palaeosols of the Sugarloaf Quarzite are the gypsic profiles of the 3.2 Ga Moodies Group of the Barberton area of South Africa (Nabhan *et al.*, 2016). Also similar are barite–nahcolite profiles of the 3.0 Ga Farrel Quarzite (Retallack *et al.*, 2016) and 3.5 Ga Panorama Formation (Retallack, 2018), both in the Pilbara region of Western Australia.

Palaeosols in fluvial quartzites of the 2.6 Ga Carbon Leader of the Witwatersrand Group near Johannesburg (South Africa) are thin and green–grey, and their filamentous structures (*Thucomyces lichenoides*, *Witwatermomyces conidiophorus*) are carbonaceous and gold encrusted (Prashnowsky & Schidlowski, 1967; Hallbauer *et al.*, 1977; MacRae, 1999; Minter, 2006). Unlike quartz–rich and deeply weathered palaeosols of the Sugarloaf Quartzite, Witwatersrand palaeosols were neither oxidized nor salty (Minter, 2006; Mossman *et al.*, 2008). Palaeosols similar to

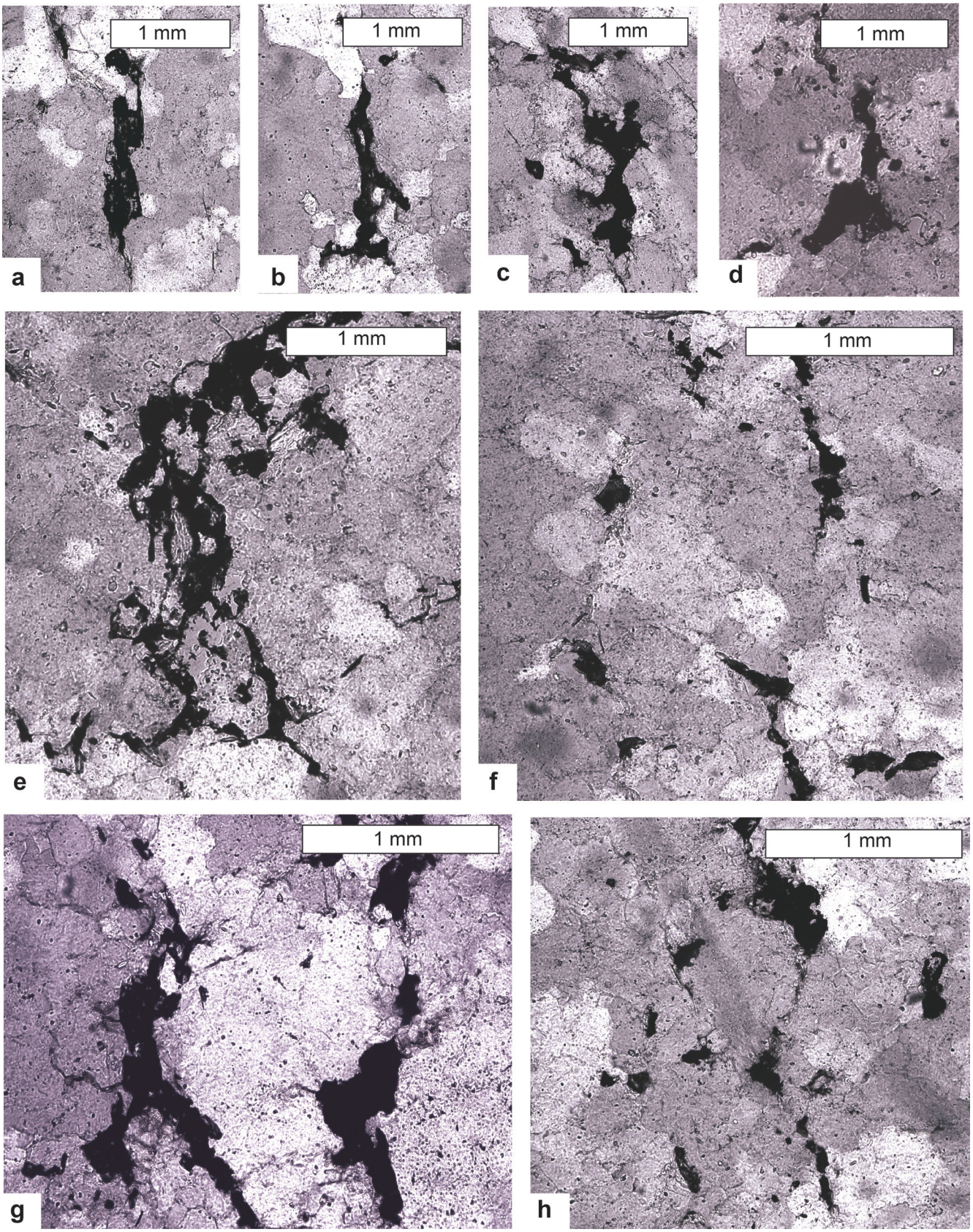

Fig. 8—Thin sections cut perpendicular to bedding to show *Erythronema ramosum* (A–E) and *Erythronema robustum* (F–H). Specimen numbers (located in Fig. 4) in the Condon Collection, Museum of Natural and Cultural History, University of Oregon are R3460 (E–F), R3461 (A–D), and R3462 (G–H).

those of the Sugarloaf Quartzite also have been described from the 1.8 Ga Lochness Formation, near Mt Isa, Queensland (Driese *et al.*, 1995). Palaeosols in the fluvial Lochness Formation are red, deeply weathered, and show tubular mottles, as in Medicine and Marie pedotypes, but have no sand crystals like the Mirror pedotype. Lochness Formation palaeosols are quartz–rich, but more feldspathic and clayey than those of the Sugarloaf Quartzite, and also have complex drab–haloed filaments like those seen in Ediacaran (Retallack, 2011a, 2012b) and Cambrian palaeosols (Retallack, 2008, 2009a–b, 2011b). Homogenization of bedding by ferruginous filaments and cracks in palaeosols of the Lochness Formation is very similar to that observed in the Sugarloaf Quartzite. Most similar to palaeosols of the Sugarloaf Quartzite are palaeosols of the 1.9 Ga Stirling Range Formation of Western Australia, particularly the Kumbar and Wiluk pedotypes, with similar diffuse, subsurface (By) horizons of pseudomorphed gypsum sand crystals (Retallack & Mao, 2019).

Younger Precambrian sediment–hosted palaeosols are known from 1.1 Ga North Shore Volcanic Group, Minnesota (Mitchell & Sheldon, 2009), the 0.6 Ga Nuccaleena Formation of South Australia (Retallack, 2011a), 0.6 Ga Ranford Formation of Western Australia (Retallack, 2020), and 0.55 Ga Ediacara Member of South Australia (Retallack, 2012b). North Shore palaeosols are in basaltic volcaniclastic and Nuccaleena palaeosols in dolomitic parent materials, unlike the Sugarloaf Quartzite. Muru palaeosols of the Ediacara Member and Thamberalg palaeosols of the Ranford Formation have large (2 cm) stellate sand crystals unlike those of the Sugarloaf Quartzite.

Comparable soils

Soils with subsurface gypsum crystals (By horizons) like Mirror palaeosols are Gypsids in the US taxonomy (Soil Survey Staff, 2014), and Gypsic Xerosols in the Food and Agriculture Organization (1974) World Map of soils. The palaeosols qualify as Xerosols rather than Yermosols because of the extent of ferruginization and destruction of primary bedding in the surface (A horizon). Such soils are known from Pleistocene and early Holocene land surfaces in Israel's Negev Desert (Dan & Yaalon, 1982) and Chile's Atacama Desert (Navarro–González *et al.*, 2003), but acid–sulfate soils with shallow water tables are rarely found in subhumid regions (Jennings & Driese, 2014; Benison & Bowen, 2015).

Interpreted soil palaeoenvironments

Generally weak to moderate development of the palaeosols (Fig. 3) is evidence of an active sedimentary palaeoenvironment (Retallack, 1991, 1997). The most developed palaeosols have gypsum sand–crystal pseudomorphs occupying about 5% by volume of the By horizon (Fig. 2E–F). In the Arena Valley of Antarctica, the development of salt stage III of gypsum nodules larger than 2 mm spanning less than 20% surface area takes 18–90 kyrs and a weakly cemented pan more than 250 kyrs (Bockheim, 1990; Retallack *et al.*, 2001). Such a frigid climate is unlikely for the Sugarloaf Quartzite, judging from REE and bulk chemical studies (Crichton & Condie, 1993). A more suitable modern analog is the relationship between gypsum abundance (*G* in area %) and geological age (*A* in kyrs) in the Sinai and Negev Deserts of Israel (Dan *et al.*, 1973; Yaalon *et al.*, 1982), given by the following equation ($R^2 = 0.95$, standard error ± 15 kyr.).

$$A = 3.987G + 5.774 \quad \text{— equation 3}$$

Using this relationship the average length of soil formation of Mirror palaeosols was 43 ± 11 kyr, and the total time represented by palaeosols in the measured section 197 kyr. This time of accumulation can be used to calculate sediment accumulation rates once original sediment depths (*Ds*) are estimated from current rock depths (*Dp*) using a standard compaction formula for Aridisols (Sheldon & Retallack 2001) and the known burial depth (*K* in km) of about 4.2 km for the Sugarloaf Quartzite (Chamberlain, 1998; Chamberlain *et al.*, 1993), as follows.

$$Ds = Dp/[-0.62/(e^{\frac{0.38}{0.27K}} - 1)] \quad \text{— equation 4}$$

From this equation, the 20.2 m measured section was originally 26.5 m thick, and sediment accumulation rate estimated from Mirror palaeosols was 0.13 mm.yr^{-1}. Durations of Marie and Medicine pedotypes were less than this, and assuming 100 and 1000 years for them, as reasonable for comparable modern Entisols and Inceptisols (Retallack, 1997), the duration of the section becomes 210 kyr and sediment accumulation rate 0.12 mm.yr^{-1}. Such rates are lower than average for millennial time scales, but far from the lowest known (Sadler, 1981). Low rates of sediment accumulation would have allowed more profound weathering, and so are compatible with textural and mineralogical maturity of the Sugarloaf Quartzite (Crichton & Condie, 1993).

Shallow water tables in a coastal deflation plain or alluvial floodplain are indicated by grey colors of palaeosol subsurface horizons and high proportions of ferrous iron in the palaeosols (Fig. 3). Intensity of oxidation decreases down profile within the palaeosols as is typical of groundwater gleization, a process in which oxidation is inhibited by standing water and organic matter for a part of the year (Retallack, 1997). Standing water dissolves soil salts and is incompatible with gypsum precipitation in soils (Dan & Yaalon, 1982). Gypsum sand–crystals are largely within red portions of palaeosols that presumably remained freely drained.

The parent material of the palaeosols was chemically and texturally mature quartz sand, augmented in silica by diagenetic–metamorphic–hydrothermal alteration (Chamberlain, 1998). Low potash and a distinct negative Eu–anomaly in rare earth element abundances of the Sugarloaf Quartzite have been used by Crichton & Condie (1993) as evidence that source terrains were deeply weathered, and that

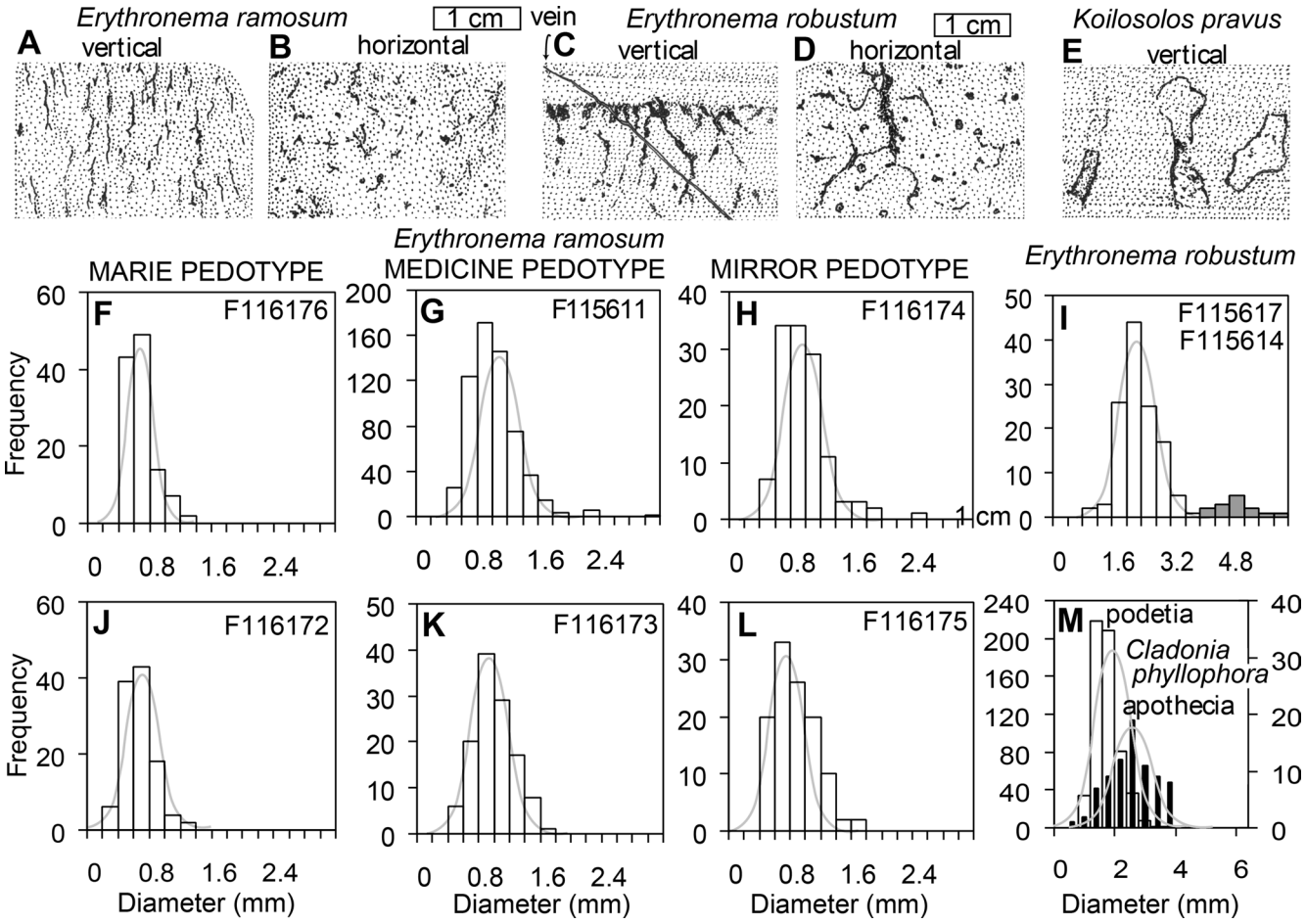

Fig. 9—Size distributions of problematic megafossils from Mirror Lake Wyoming, and a modern lichen (*Cladonia phyllophora*) from Fishtrap Lake, Montana. Light grey curves are computed normal distributions for comparison. All except apothecia of *Cladonia* (filled bars) are not normal, but log–normal (Table 4), as expected of indeterminate growth. Size increases of megafossils with degree of development of the palaeosols is suggestive of very slow growth. Specimen numbers of sketches are (a–b) F115611, (c) F115617, (d) F115606, (e) F115614.

climate had ameliorated considerably since earlier glacial conditions inferred from diamictites of the Headquarters Formation. It is also likely that compositional maturity comes from physical abrasion and recycling in coastal sand dunes and beaches (Karlstrom *et al.*, 1983). Similarly, Oregon beach sands are unusually rich in quartz considering many local basaltic headlands (Komar & McManus, 1999). The most important contributor to this thorough weathering, however, was acid–sulfate weathering, probably at pH as low as 3, and evident from abundant gypsum crystals (Bowen & Benison, 2009; Jennings & Driese, 2014; Benison & Bowen, 2015). Acid–sulfate weathering, as a supplement to carbonic–acid hydrolysis, may have been more widespread during the Palaeoproterozoic and Archaean than currently (Nabhan *et al.*, 2016, Retallack *et al.*, 2016; Retallack, 2018).

Gypsic soils comparable with Mirror palaeosols are known from arid regions of low biological productivity today (Dan & Yaalon, 1982; Ewing *et al.*, 2006; Navarro–González *et al.*, 2003), but high water–tables in Sugarloaf Quartzite palaeosols inferred above suggest that a better analog is with acid sulfate lakes which extend from arid to subhumid climates (Bowen & Benison, 2009; Jennings & Driese, 2014; Benison & Bowen, 2015). The deeply weathered nature of the Sugarloaf Quartzite (Crichton & Condie, 1993) is supported by geochemical proxies for palaeoclimate from palaeosols. Palaeoprecipitation can be gained from the palaeohyetometer of Sheldon *et al.* (2002), using chemical index of alteration without potash ($C = 100 \cdot mAl_2O_3/(mAl_2O_3 + mCaO + mNa_2O)$, in moles), which increases with mean annual precipitation (P in mm) in modern soils ($R^2 = 0.72$; S.E. = ± 182 mm), as follows.

$$P = 221e^{0.0197C} \quad \text{— equation 5}$$

This formulation is based on the hydrolysis equation of weathering, which enriches alumna at the expense of lime, magnesia, potash and soda. Magnesia is ignored because not significant for most sedimentary rocks, and potash excluded because it can be enriched during deep burial alteration of sediments (Maynard, 1992; Sheldon & Tabor, 2009). A useful palaeotemperature proxy for palaeosols devised by Sheldon *et al.* (2002) is alkali index ($N = (K_2O+Na_2O)/Al_2O_3$ as a molar

ratio), which is related to mean annual temperature (T in °C) in modern soils by equation 8 ($R^2 = 0.37$; S.E. = ± 4.4°C).

$T = –18.5N + 17.3$ — equation 6

Application of these equations to palaeosols of the Sugarloaf Quartzite give mean annual precipitation of 1287 ± 182 mm and 1331 ± 182 mm, and mean annual temperature of 10.1 ± 4.4 °C and 11.1 ± 4.4 °C for two Mirror palaeosols.

ENIGMATIC TUBULAR FOSSILS

The palaeosol interpretation advanced above, and a variety of new observations on what kind of fossils they represent, allow reassessment of the variety of tubular filamentous structures described by Kauffman & Steidtmann (1981) and herein (Figs 7–9).

Palaeosol context

Abundant, red–stained, tubular filamentous structures described by Kauffman & Steidtmann (1981) are integral to destruction of bedding within the palaeosols and also truncated by palaeosol tops. These filaments branch and taper downward in a manner analogous to fossil roots used to identify Phanerozoic palaeosols (Retallack, 1997). Kauffman & Steidtmann (1981) interpreted these tubular structures as marine trace fossil assemblages showing different degrees of bioturbation, as in the ichnofabric index of Droser & Bottjer (1986), but that interpretation is not compatible with evidence for soil formation. Increased density of burrows in marine sediments is directly analogous to burrows and roots in soils, but marine bioturbation does not show coordinated changes in color, grain–size, chemical composition, and sand crystal density and size seen in the Sugarloaf Quartzite (Figs 4–6).

Trace or body fossils, or pseudofossils?

Some of the questions posed by Palaeoproterozoic megafossils (Cloud *et al.*, 1980, 1983) are resolved by new observations supporting the idea that some of them were body fossils, not trace fossils. First among lines of evidence for this is the concertina outline and variation in width along the length of tubular structures within a matrix of texturally uniform sand (Figs 7C–D, 8). Interstitial animals may squeeze through narrow channels between soil clods and coarse sediment grains, but burrowing animals in uniform sandy sediment maintain a characteristic peristaltic–maximum cross–sectional area that is resistant to burial compaction (Seilacher, 2007). Second, the walls of tubular features are a mix of hematite, fuchsite and sericite (Crichton & Condie, 1993), very different from the sandy matrix (Fig. 8). Burrows can be lined with clay, mucus or other materials (Seilacher, 2007), but this cannot explain comparable materials in thin ramifying filaments too narrow for the passage of an animal capable of producing or moving large amounts of mucus or clay. Third, the tubular features branch irregularly outward and downward from growth centres and surfaces (as documented by Kauffman & Steidtmann, 1981), comparable with roots of vascular land plants (Retallack, 1997), colonies of soil slime molds (Stephenson & Stempen, 1994), rhizomorphs of fungi and lichens (Brodo *et al.*, 2001; Mihail & Bruhn 2005), and holdfasts of algae (Graham *et al.*, 2009). Regardless of biological affinities, these analogs are all sessile, continuously growing, organic bodies rather than transient rearrangements of silicate grains by passing animals.

Other Palaeoproterozoic megafossils have been disputed as weathering or biological structures, such as termite galleries introduced into the rocks long after their deposition (Cloud *et al.*, 1980; Seilacher, 2007). However, both scree and bedrock in this high–altitude glacial cirque are little weathered (Fig. 2A). The structures are tubular, disrupt prior bedding and are truncated by overlying beds (Figs 7A, 8, 9C). Furthermore, the tubular structures are also truncated by metamorphic veins (Figs 7A, 9C; Runnegar & Fedonkin, 1991) radiometrically dated at 1,780–1,620 Ma (Karlstrom *et al.*, 1983; Houston *et al.*, 1992; Jones *et al.*, 2010). The tubular features are thus pre–metamorphic, indigenous to the rock, and formed between intervals of sedimentation.

Other Palaeoproterozoic megafossils have been disputed as abiogenic sedimentary structures such as nodules, gas escape or bubble structures (Cloud *et al.*, 1983; Hofmann, 1991a; Seilacher, 2007). However, the Sugarloaf tubular structures taper and branch downward, not upward through bedding planes. They neither deform laminae, nor connect to surface cones, like those of water or gas escape structures (Cloud *et al.*, 1983; Frey *et al.*, 2009). The log–normal size distribution of most of the fossils (Fig. 9) distinguishes them from nodules, concretions, and mineral growths, as demonstrated by Kauffman & Steidtmann (1981). Unlike downward branching trace fossils such as *Chondrites* (Häntzschel, 1975), their thickness, branching rate, and angles of branching vary dramatically. Unlike borings such as *Clinolithes* (Häntzschel, 1975), there is no clear truncation of original grains, although metamorphic augmentation of grains cuts through the walls of the fossils (Fig. 8). Unlike pyrolusite dendrites, the fossils are not confined to planar cracks and do not show sequential crystals of constant size and shape (Fig. 8).

Fedonkin & Runnegar (1991) suggested that comparable Medicine Peak Quartzite fossils may have been metamorphic fluid evasion structures. However, the Sugarloaf Quartzite structures are truncated by metamorphic quartz veins (Figs 7A, 9C), like the Medicine Peak Quartzite specimen in the Smithsonian Institution (USNM 243015 illustrated by Kauffman & Steidtmann 1981, text–fig. 1A). No hematite was observed within the quartz veins, and it is unlikely that hematite could survive conversion to magnetite during amphibolite and granitization temperatures producing quartz veins (Thompson, 1972).

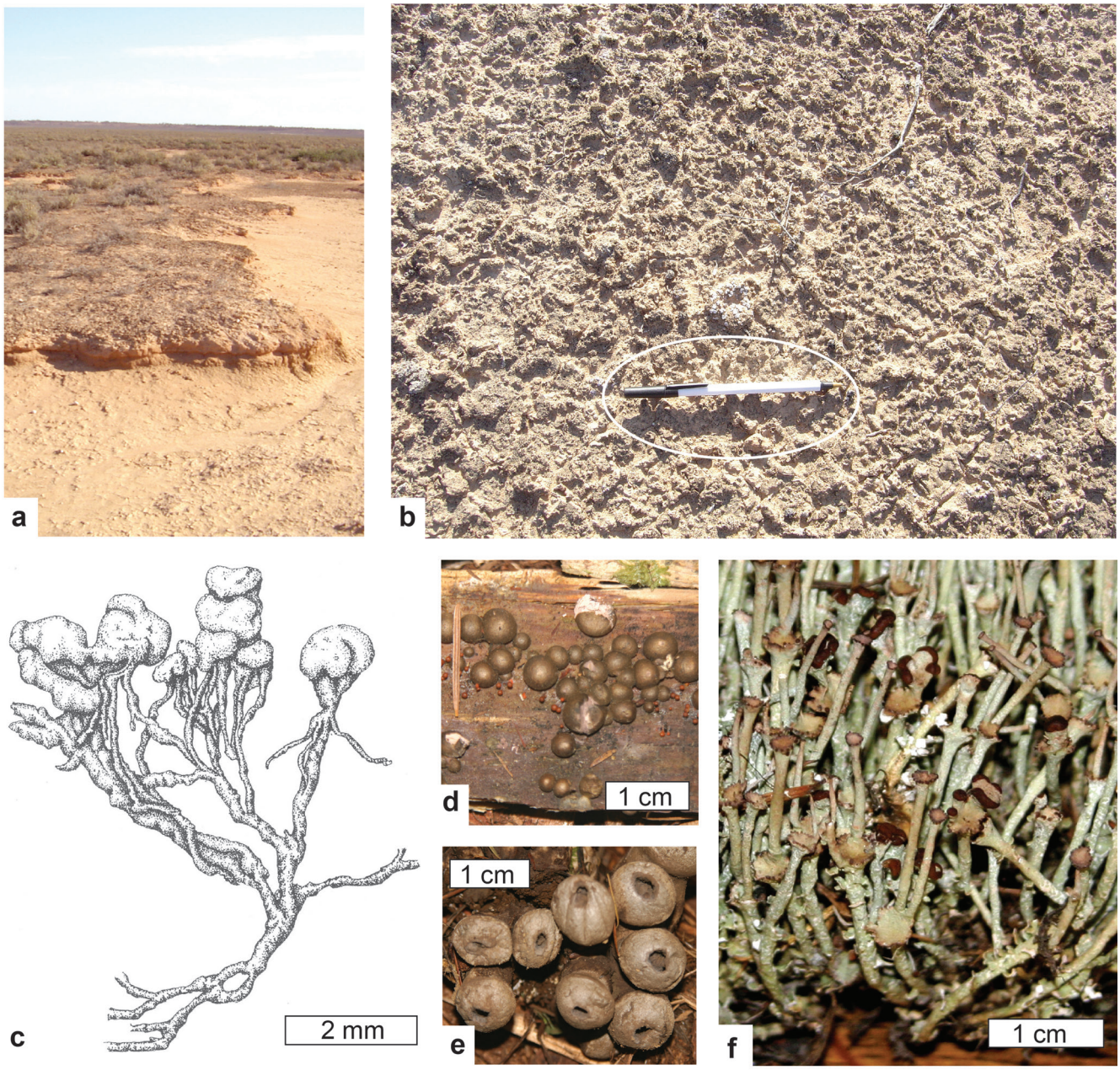

Fig. 10—Plausible modern analogs for Palaeoproterozoic megafossils. (a–b), overview of gypsic–calcareous soil (a) and detail of surface (b) of microbial earth at Lake Mungo, New South Wales (Australia), vascular plants in the background include *Atriplex nummularia* and *Maireana pyramidata*, but ground cover is largely lichens and cyanobacteria: (c), bruised lichen (*Toninia sedifolia*, Fungi, Ascomycota, Lecanorales) from Austrian Alps (after Poehlt & Baumgärtner, 1964): (d), wolf's milk slime mold (*Lycogala epidendrum*, Amoebozoa, Mycetozoa, Liceida) on bark from Hendricks Park, Eugene, Oregon: (e), pear–shaped puffball (*Morganella pyriformis*, Fungi, Basidiomycota, Agaricales) from Eugene, Oregon: (f), fruticose lichen (*Cladonia phyllophora*, Fungi, Ascomycota, Lecanorales) from Fishtrap Lake, Montana. Pen 18 cm long for scale is in white ellipse of (b).

SYSTEMATIC PALAEONTOLOGY

Form taxonomy

Kauffman & Steidtmann (1981) recognized 9 distinct tube morphologies in the Medicine Peak Quartzite, but only three are recognized in the new material from the Sugarloaf Quartzite described below. Biological affinities of these megafossils are uncertain at the kingdom level, so that the new taxa proposed here are form genera in the palaeobotanical provisions of the International Code of Botanical Nomenclature (Turland *et al.*, 2018). Form species acknowledge preservational styles with different names, and thus multiple epithets for the same biological

species (Retallack & Dilcher, 1988; Nishida *et al.*, 2007). This cumbersome system allows uncertainty concerning biological affinities and mosaic evolution of different plant organs, while addressing shortcomings of different styles of preservation, and preserving taxonomic rigor. Root trace and dispersed pollen names are separate parataxonomies, of ichnology (Häntzschel, 1975) and palynology, respectively (Traverse, 1988).

Erythronema gen. nov.

(Figs 7A–E, 8, 9A–D)

Type species— *Erythronema ramosum* sp. nov.

Derivation— The new genus is from έρυθρος (Greek adjective, red) and νημα (Greek, neuter) for thread.

Diagnosis— Narrow (< 4 mm diameter), tubular features of highly variable diameter and irregular branching; abruptly ending at the top, but radiating, tapering, and irregularly branching downward across lamination, and outward from growth centres; lacking bundles or fibres, internally differentiated tissue zones, or recognizably cellular outer surfaces. Preserved as tubular features defined by irregular hematite–stained phyllosilicates within quartz sandstones.

Comparisons—As noted by Kauffman & Steidtmann (1981), *Erythronema* is superficially like vascular plant root traces. The palaeobotanical form genus *Radicites* (Potonié, 1893) includes carbonaceous root remains, as well as drab–haloed root traces in red palaeosols, such *as Radicites erraticus* (Arafiev & Naugolnykh, 1998; Yakimenko *et al.*, 2004). *Radiculites* (Lignier, 1906) is a fossil root with permineralized xylem, but even *Radicites* betrays woody fibrous centers (steles) not seen in hollow *Erythronema*. Furthermore, vascular plant roots have a much wider range of orders of branches from meter–scale tap roots to micron–scale root hairs (Retallack, 1997). *Rhadix* (Fritsche, 1908) is a tubular fossil (Arafiev & Naugolnykh, 1998) much stouter than *Erythronema*. Other filamentous structures are known from the upper parts of palaeosols from the 1.8 Ga Lochness Formation, near Mt Isa, Queensland (Driese *et al.*, 1995) and from the Cambrian Billys Creek, Moodlatana, Balcoracana, Pantapinna, and Grindstone Range Formations of the eastern Flinders Ranges, South Australia (Retallack, 2008). These are green–grey filaments in clayey red palaeosol matrix, assigned to form genus *Prasinema* (Retallack, 2011b), not red in grey sandy matrix like *Erythronema*. These rootlike body fossils are much more irregular in form and branch more copiously than the ichnogenus *Palaeophycus*, which has been compared with remains of *Erythronema* from the Medicine Peak Quartzite by Kauffman & Steidtmann (1981).

Two species of *Erythonema* are recognized here for narrow (1–2 mm) and wide (2–4 mm) forms, corresponding with sizes typical for rope–forming cyanobacteria (Garcia–Pichel & Wojciechowski, 2009) and fungal cords (Mihail & Bruhn, 2005), respectively. These sizes for the fossils are distinct and convenient (Fig. 9), but as for form species in general, do not imply that their biological affinities are known.

Erythronema ramosum sp. nov.

(Figs 7A, C, 8A–E, 9A–B)

Synonymy—1981, "burrow–like tube morphology 9", Kauffman & Steidtmann, text–figs. 5, 6E.

Holotype— Condon Collection, Museum of Natural and Cultural History, University of Oregon specimen F115611 loose on slope near Mirror Lake, Wyoming (locality L2491): Palaeoproterozoic, Sugarloaf Quartzite.

Derivation— The epithet *ramosus* (Latin adjective) means branching.

Diagnosis—Erythronema with narrow (1–2 mm) tubular structures, copiously branching outward and downward.

Comparisons—The only other species, *Erythronema robustum* defined below, has wider tubular structures than *E ramosum*. Both species are hollow, walled structures. This hollow structure is not obvious in hand specimens, but apparent from thin sections of *E. ramosum* (Fig. 8A–E). Other problematic megafossils in the Medicine Peak Quartzite differ in having bulbous expanded terminations, back fill structures, wall linings and strongly contrasting fills (types 1–8 of Kauffman & Steidtmann 1981), which were not seen in large collections from the Sugarloaf Quartzite made for this study.

Measurements—Lengths of *Erythronema ramosum* are difficult to measure accurately because tubes curve and branch in all directions from surfaces of hand specimens and thin sections. Lengths may be as much as the 10–40 cm bioturbated upper part of the palaeosols, because the tubes appear continuous from the surface (Fig. 4). The holotype of *K. ramosum* has tube diameters with the following dimensions: mean of 0.81 mm with standard deviation ± 0.30 mm, median 0.78 mm, mode 0.63 mm, range 0.22–2.85 mm, for 600 measurements (see also Tables 4–5).

Erythronema robustum sp. nov.

(Figs 7B, E, 8F–H, 9C–D)

Synonymy—1981, "burrow–like tube morphology 1", Kauffman & Steidtmann, text–figs 5, 6H–I, 7, 8, 10.

Holotype— Condon Collection, Museum of Natural and Cultural History, University of Oregon, specimen F115617, found loose on slope near Mirror Lake, Wyoming (locality UO12491): Palaeoproterozoic, Sugarloaf Quartzite.

Derivation— From *robustus* (Latin adjective) meaning stout.

Diagnosis—Erythronema with wide (2–4 mm) tubular structures, branching irregularly and at long intervals, outward and downward.

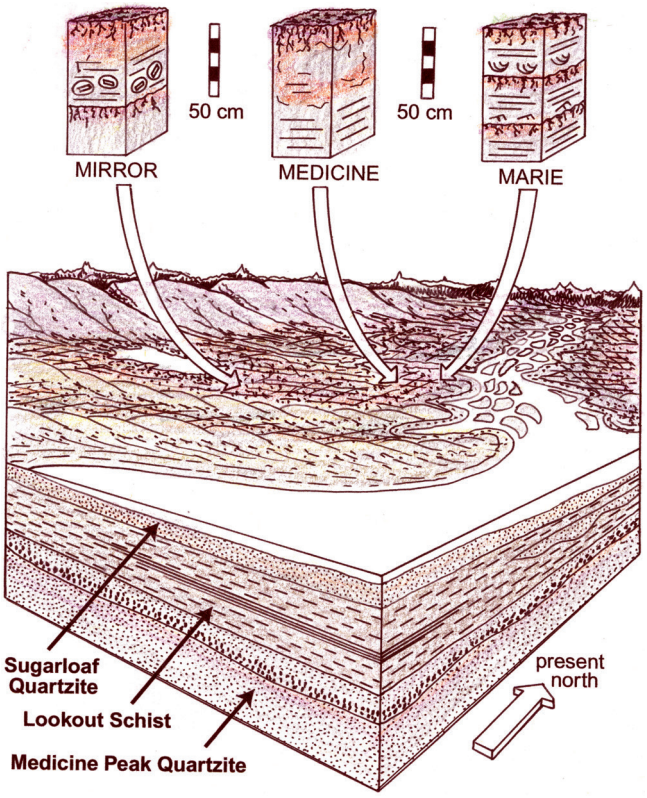

Fig. 11—Hypothetical reconstruction of life, soil and sedimentary environments during deposition of the lower Sugarloaf Quartzite near modern Medicine Bow Peak, Wyoming. Lithological symbols are as for Figs 3–4.

Comparisons—Erythronema robustum is wider than *E. ramosum* and also less copiously branched, with less distinct walls. Terminal bends and swellings were not seen, nor special linings, nor backfill structures (as in types 2–8 of Kauffman & Steidtmann 1981). A specimen with internal layering superficially similar to back fills is illustrated here (Fig. 7B), but these layers are a continuation of bedding from the exterior. These layers are puzzling unless the organisms grew in sediment.

Measurements— Lengths of *Erythronema robustum* like those of *E. ramosum* pass in and out of hand specimen surfaces and thin sections, but appear shorter than for *E. ramosum*, probably only 10–20 cm of the bioturbated upper part of Marie and Medicine palaeosols (Fig. 4). The holotype of *E. robustum* has tube diameters with the following dimensions: mean of 1.94 mm with standard deviation ± 0.50 mm, median 1.86 mm, mode 1.45 mm, range 0.75–3.32 mm, for 123 measurements (see also Tables 4–5).

Koilosolos gen. nov.

(Figs 7F, 9E)

Type species— *Koilosolos pravus* sp. nov.

Derivation— The new genus is from κοιλος (Greek adjective) for hollow, and σολος (Greek, masculine) for a lump or mass of iron (as used in athletic competitions).

Diagnosis— Globose broadly wrinkled hollow structure above subvertical hollow tubular structures, flaring or branching downward and no more than half the diameter of the globose structure: defining wall structures lack cellular structure. Preserved as hematite–stained phyllosilicate outlines within quartz sandstone.

Comparisons—When first discovered *Koilosolos* was assumed to be a specimen of a vase–shaped fossil (type 7 of Kauffman & Steidtmann 1981), which they compared with the trace fossil *Diplopichnus gulosus*, and considered burrows of predatory cnidarians such as *Cerianthus*. Their specimen was lost in the field during the winter of 1973, but more are needed, because our material now shows that either (1) their specimen was oriented differently, or (2) the orientation assumed by Kauffman & Steidtmann (1981) was upside–down. The specimen of this study shows an angular divergence of 21° between the base of a scour–and–fill truncating pre–existing lamination indicating that the assumed tube above the bulb was really a bulb atop a tube (Fig. 7F). This orientation also rules out comparison with the trace fossil genus *Macanopsis* and *Bergaueria* (for associated remains by Kauffman & Steidtmann 1981), which have bulbous bases to entrance tubes. *Amphorichnus* is another rounded cavity fill with a downward extension (Häntzschel, 1975), but the cavity is more ellipsoidal and regular than in *Koilosolos*, and the downward extension a mere pimple rather than a tube. The irregularity of *Koilosolos* is a striking feature. The bulb–like part is deeply creased, and the tubular base flares and buckles. The hematite–sericite wall in some places is missing as if broken or rotted, and the body of the fossil is filled with sand as if originally hollow or decayed.

Koilosolos pravus sp. nov.

(Figs 7F, 9E)

Holotype—Condon Collection, Museum of Natural and Cultural History, University of Oregon specimen F115614 loose on slope near Mirror Lake, Wyoming (locality UO12491): Palaeoproterozoic, Sugarloaf Quartzite.

Derivation—The epithet *pravus* (Latin adjective) means crooked or misshapen.

Specific diagnosis—Hollow globose structures 11.5 mm in diameter above hollow tubular structures 10–20 mm long and 3–5 mm in diameter.

Comparisons— Only a single species of *Koilosolos* is known.

Measurements—Only a single globose structure was found with maximum horizontal diameter of 11.5 mm. The holotype rock with *Koilosolos pravus* has three tubular structures with preserved lengths of 21.2, 19.9, and 31.9 mm,

and diameters with the following dimensions: mean of 4.66 mm with standard deviation ± 0.59 mm, median 4.65 mm, mode 4.70 mm, range 3.76–5.88 mm, for 15 measurements.

EARLY LIFE ON LAND

Palaeobiological interpretations

Tubular megafossils of palaeosols in the Sugarloaf and Medicine Peak Quartzites are of uncertain biological affinity, because histology and organic geochemical composition are not preserved. Their similarity to vascular plant roots and corms, and algal holdfasts is superficial. There is no trace of plant fibre (tracheids) and the widest ones are filled with sandstone as if hollow, unlike common preservation of root steles within rotted root cortex within palaeosols (Retallack, 1997). They were penetrative structures deformed around grains (Fig. 8), not free structures covered by sediment like algal holdfasts (Graham *et al.*, 2009). Also superficial are similarities with burrows of worms, or trails of molluscs, or giant amoebae thought responsible for other comparable Palaeoproterozoic megafossils (Kauffman & Steidtmann, 1981; Seilacher, 2007; Bengtson *et al.,* 2007), considering their variation in thickness, branching and fill.

Tubular features of the Sugarloaf and Medicine Peak Quartzite are most similar in their appearance and texture to microbial cords and ropes of biological soil crusts (Belnap & Lange, 2003), also known as microbial earths and polsterlands (Retallack, 1992, 2012a), which also show an overall organization of increased density toward a truncated upper surface (Fig. 10A). This is a key difference between biological soil crusts, which show intimate admixture of microbes and silicate grains (Belnap & Lange, 2003), and aquatic microbial mats, which grow above, wrinkle off, and detach in loose sheets from their silicate substrate (Seilacher, 2007). Microbial earths in contrast form radial expansions, wrinkles, dimples, and healed cracks that fold in complex ways (Fig. 10B). Many problematic fossils that have been dismissed as pseudofossils (Table 1) could profitably be reassessed from this new perspective.

Finely branching and tapering tubular structures like *Erythronema* are common in biological soil crusts, and are formed by a variety of organisms: (1) sheathed bundles of cyanobacteria, such as *Microcoleus vaginatus* (Hu *et al.*, 2002; Garcia–Pichel & Wojciechowski, 2009); (2) phaneroplasmodia and plasmodiocarps of slime molds, such as *Physarum polycephalum* and *Hemitrichia serpula* (respectively of Stephenson & Stempen, 1994); (3) rhizines of bruised lichens, such as *Toninia sedifolia* (Fig. 10C); and (4) rhizomorphs of fungi, such as *Armillaria mellea* (Mihail & Bruhn, 2005). The stout tubes and bulbous structures of *Koilosolos* are matched by fewer forms, such as (1) fruiting bodies or podetia of slime molds, such as *Lycogala epidendrum* (Fig. 10D), (2) thalli and rhizines of puffball fungi, such as *Morganella pyriformis* (Fig. 10E), and (3) thalli and rhizines of lichens (Poehlt & Baumgartner, 1964; Brodo *et al.*, 2001). Comparable modern organisms require chemical tests and spores for accurate identification, so that biological affinities of these fossils may never be known precisely.

The hollow tubular structures are comparable with vegetative podetia of the lichen *Cladonia* or morel *Morchella*, rather than solid reproductive structures (such as apothecia, Fig. 10F). However, the complex internal structures of slime mold fruiting bodies, mushrooms, morels, truffles, and apothecia could decay back to leave hollow walls, especially in the oxidizing environment indicated by palaeosol ferrous–ferric ratios (Fig. 4).

The log–normal size distribution of tubular structures, like podetia of the living lichen *Cladonia phyllophora* measured for comparison (Fig. 9M, 10F: Table 4), also supports actinobacterial, fungal or lichen vegetative affinities. Unlike metazoans, which reach a modal reproductive size and have a normal size distribution, organisms with indeterminate growth such as lichens and plants show a log–normal size distribution (Peterson *et al.*, 2003). Reproductive structures on the other hand are determinate and short–lived in their growth and show normal size distribution, as in apothecia of the lichen *Cladonia phyllophora* (Fig. 9M). Metazoan fossil assemblages can show nearly log–normal size distributions if there is unusually high infant mortality, but such cases are revealed by polymodal distributions of different age cohorts or species (Zhang *et al.*, 2007), rather than continuous log–normal distributions.

Tubular structures of the Sugarloaf Quartzite increase in density with degree of bedding destruction and size of crystal pseudomorphs (Fig. 3), like plants, lichens, fungal and actinobacterial mycelia, which are long–lived, slow–growing agents of soil formation (Retallack, 1997). In contrast, mushrooms, morels, and apothecia are short–lived reproductive phases (Mueller *et al.*, 2004). Slime mold aggregations also are short lived and are not as substantial or compaction resistant as the tubular structures (Stephenson & Stempen, 1994).

Few of these living organisms compared with the tubular structures have independent fossil records extending back 2200 Ma. Ediacaran and earliest Cambrian rocks have yielded plausible actinobacteria such as *Primoflagella speciosa* (Gnilovskaya, 1985). Permineralized fossils from the 3000 Ma Farrel Quartzite of Western Australia may have been actinobacterial sporangia (Retallack *et al.*, 2016). Lichenized actinobacteria may be as old as 2800 Ma in the Carbon Leader of the Witwatersrand Group near Johannesburg, South Africa (Hallbauer *et al.*, 1977; Mossman *et al.*, 2008). Slime molds are known as old as 1900 Ma in the Stirling Range Quartzite of Western Australia (Retallack & Mao, 2019), 1000 Ma in the Neryuenskaya Formation of Siberia (Hermann & Podkovryov, 2006). Glomeromycotan or Mucoromycotinan fungi may be represented by 2200 Ma *Diskagma* from the

Table 6—Palaeosols in Palaeoproterozoic Sugarloaf Quartzite of Wyoming.

Pedotype name	Diagnosis	Soil taxonomy (Soil Survey Staff 2014)	Food & Agriculture Organization (1974)	Palaeoclimate	Former biota	Palaeotopography	Parent material	Time (k.yr)
Marie	Red mottled sandstone (A) over grey bedded sandstone (C)	Psamment	Dystric Fluvisol	Not indicative	Polsterland with slender and stout tubes, and thick tubes with bulb.	Alluvial levee and point bar	Quartz sand	0.1–0.5
Medicine	Red mottled sandstone (A) over less bioturbated red sandstone (Bw) and grey bedded sandstone (C)	Ochrept	Dystric Cambisol	Not indicative	Polsterland with slender and stout tubes	Coastal deflation plain	Quartz sand	1–2
Mirror	Red mottled sandstone (A) over shallow (<32 cm) red sandstone with white quartz–haloed gypsum pseudo–morphs (By)	Gypsid	Gypsic Xerosol	Arid (151–71±129 mm mean annual precipitation), temperate (10.1–11.1±4.4 °C mean annual temperature)	Polsterland with slender tubes only	Coastal deflation plain	Quartz sand	32–54

Hekpoort Basalt of South Africa (Retallack *et al.*, 2013b), 1400 Ma *Horodyskia* from the Apekunny Argillite of Montana (Retallack *et al.*, 2013a), and 1400 Ma *Tappania* from the Wyniatt Formation of Victoria Island, Canada (Butterfield, 2005; Retallack, 2015b), and 1000 Ma *Ourasphaira* from the Grassy Bay Formation of Arctic Canada (Loron *et al.*, 2019). Permineralized fossils such as *Archaeotrichon* in the Apex Chert (3580 Ma) near Marble Bar, Western Australia (Schopf & Packer, 1987; DeGregorio *et al.*, 2009) are isotopically more like purple sulfur bacteria than cyanobacteria (Retallack *et al.*, 2016). Cyanobacteria and photosystem 2 may be only as old as 2200 Ma (Kirschvink & Kopp, 2008). Cyanobacteria may be represented by sheath microfossils (*Siphonophycus*) as old as 2500 Ga, but were diverse by 2000 Ma (Sergeev, 2009). Given the carbon–lean and oxidized composition of the Sugarloaf Quartzite palaeosols cyanobacterial ropes are an attractive explanation for *Erythronema ramosa*, fungal cords for *Erythronema robusta*, and glomeromycotan vesicles a plausible explanation for *Koilosolos*.

Palaeoecological interpretations

Although the exact biological nature of tubular Palaeoproterozoic terrestrial fossils remains uncertain, several aspects of their general appearance and ecology can be inferred from the palaeosols. In the classification of Retallack (1992) these would have been polsterlands, because they included megascopic microbial consortia (globules and stout tubules), rather than entirely microscope life of microbial earths. Fossils of the Sugarloaf Quartzite present a view of Palaeoproterozoic (200 Ma) polsterlands (Fig. 11) as an oligotrophic ecosystem with at least two demonstrated limitations, in addition to theoretical limitations such as low oxygen, and thus low ozone and high ultraviolet radiation, widely regarded as limiting early life on land (Cockell & Raven, 2007).

First, these ecosystems colonized very low nutrient substrates: alkalies and alkali earths in these palaeosols total only 0.14 ± 0.12 weight percent (mean and 2 standard

deviations from analyses of Table 2). Feldspar contents are not more than 5 volume % (Table 3). This was a deeply weathered (Crichton & Condie, 1993), and low nutrient substrate (Retallack, 1997).

Second, abundant ferrous iron and high chroma mottles are evidence of seasonally high water–tables in an unstable sedimentary environment (Retallack, 1997). Cyanobacteria (Hu *et al.*, 2002; Garcia–Pichel & Wojciechowski, 2009) and other soil crust organisms (Belnap & Lange, 2003) are known to stabilize desert soils against eolian and fluvial erosion. For this Palaeoproterozoic ecosystem seasonal stabilization may also have come from water saturation, as in deflation plains of coastal dune–fields today, which also are sparsely vegetated compared with surrounding coppice dunes (Riksen & Goossens, 2007). A better modern analog are acid sulfate lakes, with a diverse microbiome, but no obvious vascular plants (Bowen & Benison, 2009; Benison & Bowen, 2015).

For these reasons, the palaeosols and megafossils of the Sugarloaf Quartzite are unlikely to have been the most productive ecosystems with the highest biomass for their time. Other Precambrian sediment–hosted palaeosols with life–like physical structures are known from the1800 Ma Lochness Formation, near Mt Isa, Queensland (Driese *et al.*, 1995), the 2200 Ma Hekpoort Basalt near Waterval Onder, South Africa (Retallack *et al.*, 2013a), and the 2800 Ma Carbon Leader of the Witwatersrand Group near Johannesburg, South Africa (Prashnowsky & Schidlowski, 1967; Hallbauer *et al.*, 1977; MacRae, 1999; Minter, 2006; Mossman *et al.*, 2008). These palaeosols have neither the gypsic horizons like Sugarloaf Quartzite palaeosols, nor calcic horizons of South Australian Cambrian–Ediacaran palaeosols (Retallack, 2008, 2012b), and so were not limited by water. Isotopically light organic carbon of presumed photosynthetic origin has been reported in a 800 Ma palaeosol below the Torridonian Supergroup in Scotland (Retallack & Mindszenty, 1994), on 1300 Ma palaeokarst in the Mescal Limestone of Arizona (Beeunas & Knauth, 1985; Vahrenkamp *et al.*, 1987), and from a 2300 Ma palaeosol below the Huronian Supergroup near Elliott Lake, Ontario (Mossman & Farrow, 1992). Remarkably light C isotope values indicative of methanotrophs have been recorded from the 2800 Ma Mt Roe palaeosol of Western Australia (Rye & Holland, 2000) and 3000 Ma Farrel Quartzite palaeosols of Western Australia (Retallack *et al.*, 2016). Isotopically heavy C–isotope values like those of hypersaline microbes are known from the 2600 Ma Schagen palaeosol South Africa (Watanabe *et al.*, 2000, 2004). More general arguments for Precambrian life on land back at least to 800 Ma have come from complex clays (Kennedy *et al.*, 2006) and carbonate isotopic compositions (Knauth & Kennedy, 2009). The fossils described here are not the only evidence for Precambrian life on land, but allow megascopic visualization of life and landscapes of the early Earth (Fig. 11).

CONCLUSIONS

Metazoans are conventionally considered to have arisen during the Ediacaran (Cloud *et al.*, 1980, 1983; Gaidos *et al.*, 2007; Maloof *et al.*, 2010, 2011), and metazoans in pre–Ediacaran rocks remain controversial (Neuweiler *et al.*, 2009; Planavsky *et al.*, 2009). Some Ediacaran body fossils could be lichens or other microbial colonies (Retallack, 2007, 2009a; Fedonkin *et al.*, 2008), and "animal embryos" are more likely mesomycetozoan protists (Huldtgren *et al.* 1990). *Cloudina*, and other tubular fossils of "latest Ediacaran Wormworld" are more convincing metazoans (Schiffbauer *et al.*, 2016). This study now introduces two new concepts to this controversial topic, with study of a new assemblage of megafossils from the 2200 Ma Sugarloaf Quartzite of the Medicine Bow Range, Wyoming. These particular megafossils may be (1) body fossils rather than trace fossils, and (2) terrestrial rather than marine. Ideas about enigmatic markings in sandstones and siltstones have been dominated for a long time by hypotheses of worms, polyps and jellyfish leaving their mark on marine sands and silts (Table 1). This study introduces an array of non–marine alternative hypotheses including trace and body fossils of rope–forming cyanobacteria, lichens, fungi, and slime molds (Figs 8–9).

The biological affinities of these fossils remain problematic, but a start has now been made in visualizing the general appearance of early life on land, and in describing new palaeosols that may represent physical traces of early terrestrial ecosystems. Like stromatolites (Allwood *et al.*, 2006, 2007), microbial earth palaeosols give ecosystem–scale insights into early life. Other evidence for Precambrian life on land now comes from clay mineralogy (Kennedy *et al.*, 2006), organic geochemistry (Prashnowsky & Schidlowski, 1967; Hallbauer *et al.*, 1977), and isotopic geochemistry (Retallack & Mindszenty, 1994; Rye & Holland, 2000; Watanabe *et al.*, 2000, 2004; Knauth & Kennedy, 2009). Precambrian pedofabrics and tubular fossils like those described here are widespread (Driese *et al.*, 1995; Mossman *et al.*, 2008; Mitchell & Sheldon, 2009; Retallack, 2011a; Retallack & Mao, 2019). Wider recognition of similar features may reveal better preserved and biologically informative examples.

Acknowledgements*—Dima Grazhdankin and Erle Kauffman offered helpful discussions. Douglas Erwin helped locate specimens in the Smithsonian Institution and Edward Davis offered useful statistical advice. Jonathan Calede helped with measurements, and Winifred Kehl provided editorial help. The manuscript was greatly improved following reviews by Nora Noffke, Stefan Bengtson, Bruce Runnegar, and Santosh K. Pandey.*

REFERENCES

Allwood AC, Walter MR, Kamber BS, Marshall CP & Burch IW 2006. Stromatolite reef from the Early Archaean era of Australia. Nature 441: 714–718.

Allwood AC, Walter MR, Burch IW & Kamber BS 2007. 3.43 billion year old stromatolite reef from the Pilbara Craton of Western Australia; ecosystem scale insights to early life on Earth. Precambrian Research 158: 198–227.

Arafiev MP & Naugolnykh SV 1998. Fossil roots from the upper Tatarian deposits in the basin of the Sukhona and Malaya Severnaya Dvina Rivers: stratigraphy, taxonomy and orientation palaeoecology. Paleontological Journal 32: 82–96.

Barley ME, Dunlop JSR, Glover JE & Groves DI 1979. Sedimentary evidence for an Archean shallow water volcano–sedimentary facies, eastern Pilbara Block, Western Australia. Earth and Planetary Science Letters 43: 74–84.

Beeunas MA & Knauth LP 1985. Preserved stable isotope signature of subaerial diagenesis in the 1.2 b.y. Mescal Limestone, central Arizona: implications for the timing and development of a terrestrial plant cover. Geological Society of America Bulletin 96: 737–745.

Bekker A, Karhu JA, Eriksson KA, & Kaufman AJ 2003. Chemostratigraphy of Palaeoproterozoic carbonate successions of the Wyoming Craton: tectonic forcing of biogeochemical change? Precambrian Research 120: 279–325.

Belnap J & Lange OL (Editors) 2003. Biological soil crusts: structure, function and management. Berlin, Springer, 503 p.

Benison KC & Bowen BB 2015. The evolution of end–member continental waters: The origin of acidity in southern Western Australia. GSA Today 25: 4–10.

Ben–Jacob E, Schachnet O, Tenenbaum A, Cohen I, Czirok A & Vicsek T 1994. Generic modelling of cooperative growth patterns in bacterial colonies. Nature 368: 46–49.

Bengtson S & Rasmussen B 2009. New and ancient trace makers. Science 323: 346–347.

Bengtson S, Rasmussen B & Krapež B 2007. The Palaeoproterozoic megascopic Stirling biota. Paleobiology 33: 351–381.

Bockheim JG 1990. Soil development rates in the Transantarctic Mountains. Geoderma 47: 59–77.

Bonner JT 2009. The social amoebae. Princeton, Princeton Univ. Press, 144 p.

Bowen BB & Benison KC 2009. Geochemical characteristics of naturally acid and alkaline saline lakes in southern Western Australia. Applied Geochemistry 24: 268–284.

Branagan D 2005. T.W. Edgeworth David: a life. Canberra, National Library of Australia, 648 p.

Breyer JA, Busby AB, Hanson RE & Roy EC 1995. Possible new evidence for the origin of metazoans prior to 1 Ga: sediment–filled tubes from the Neoproterozoic Allamore Formation, Trans–Pecos Texas. Geology 23: 269–2712.

Brimhall GH, Chadwick OA, Lewis CJ, Compston W, Williams IS, Danti KJ, Dietrich WE, Power ME, Hendricks D & Bratt J 1992. Deformational mass transport and invasive processes in soil evolution. Science, 255: 695–702.

Brodo IM, Sharnoff SD & Sharnoff S 2001. Lichens of North America. New Haven, Yale Univ. Press, 828 p.

Butterfield NJ 2005. Probable Proterozoic fungi. Paleobiology 31: 165–182.

Chamberlain KR 1998. Medicine Bow orogeny: timing of deformation and model of crustal structure produced during continent–arc collision ca 1.78 Ga, southeastern Wyoming. Rocky Mountain Geology 33: 259–277.

Chamberlain KR, Patel SC, Frost R & Snyder GL 1993. Thick–skinned deformation of the Archean Wyoming province during Proterozoic arc–continent collision. Geology 21: 995–998.

Clemmy H 1978. World's oldest animal traces. Nature 261: 576–578.

Cloud PE, Gustavson LB & Watson JAL 1980. The works of living social insects as pseudofossils and the age of the oldest known Metazoa. Science 210: 1013–1015.

Cloud P, Kauffman EG & Steidtmann JR 1983. Are these the oldest metazoan trace fossils? discussion and reply. Geology 11: 618–621.

Cockell CS & Raven JA 2007. Ozone and life on the Archaean Earth. Philosophical Transactions of the Royal Society London A365: 1889–1901.

Crichton JG & Condie KC 1993. Trace elements as source indicators in cratonic sediments: a case study from the early Proterozoic Libby Creek Group, southeastern Wyoming. Journal of Geology 101: 319–332.

Dan J & Yaalon DH 1982. Automorphic saline soils in Israel. *In*: Yaalon DH (Editor)─ Aridic soils and geomorphic processes. Catena, Braunschweig: 103–115.

Dan J, Moshe R & Alperovich N 1973. The soils of Sede Zin. Israel Journal of Earth Sciences 22: 211–227.

David TWE & Tillyard RJ 1936. Memoir of the fossils of the late Pre–Cambrian (lower Proterozoic) from the Adelaide Series, South Australia. Sydney, Angus and Robertson, 112 p.

de Gregorio BT, Sharp TG, Flynn GJ, Wirick S & Hervig RL 2009. Biogenic origin for Earth's oldest putative megafossils. Geology 37: 631–634.

Dong L, Xiao SH, Shen B, Yuan X–L, Yan X–Q & Peng YB 2008. Restudy of the worm–like carbonaceous compression fossils *Protarenicola*, *Pararenicola*, and *Sinosabellidites* from early Neoproterozoic successions on North China. Palaeogeography Palaeoclimatology Palaeoecology 258: 138–161.

Driese SG, Simpson E, & Ericksson KA 1995. Redoximorphic palaeosols in alluvial and lacustrine deposits, 1.8 Ga Lochness Formation, Mt Isa: pedogenic processes and implications for paleoclimate. Journal of Sedimentary Research A66: 58–70.

Droser ML & Bottjer DJ 1986. A semiquantitative field classification of ichnofabric. Journal of Sedimentary Petrology 56: 558–559.

El Albani A, Bengtson S, Canfield DE, Bekker A, Machiarelli R, Mazurier A, Hammarlund EU, Boulvais P, Dupuy J–J, Fontaine C, Fürsich FT, Gauthier–Lafaye F, Janvier P, Javaux E, Ossa FO, Pierson–Wickmann AC, Ribolleua A, Sardini P, Vachard D, Whitehouse M & Meunier A 2010. Large colonial organisms with coordinated growth in oxygenated environments 2.1 Gyr ago. Nature 466: 100–104.

El Albani A, Mangano MG, Buatois LA, Bengtson S, Riboulleau A, Bekker A, Konhauser K, Lyons T, Rollion–Bard C, Bankole O, Baghekema SGL, Meunier A, Trentesaux A, Mazurier A, Aubineau J, Laforest C, Fontaine C, Recourt P, Fruh EC, Macchiarelli R, Reynaud JY, Gauthier–Lafayek F & Canfield DE 2019. Organism motility in an oxygenated shallow–marine environment 2.1 billion years ago. U.S. National Academy of Sciences. Proceedings 116;3431–3436.

Ewing SA, Sutter B, Owen J, Nichizumi K, Sharp W, Cliff SS, Perry K, Dietrich W, McKay CP & Amundson R 2006. A threshold in soil formation at Earth's arid–hyperarid transition. Geochimica Cosmochimica Acta 70: 5291–5322.

Faul H 1949. Fossil burrows from the Pre–Cambrian Ajibik Quartzite of Michigan. Nature 164: 32.

Faul H 1950. Fossil burrows from the Precambrian Ajibik Quartzite of Michigan. Journal of Paleontology 24: 102–106.

Fedonkin MA & Runnegar B 1991. Proterozoic metazoan trace fossils. *In*: Schopf JW & Klein C (Editor)─The Proterozoic biosphere: a multidisciplinary study. Cambridge Univ. Press, Cambridge, p. 389–395.

Fedonkin MA, Gehling JG, Grey K, Narbonne GM & Vickers–Rich P 2008. The rise of animals: evolution and diversification of the Kingdom Animalia. Baltimore, Johns Hopkins Univ. Press, 344 p.

Fenton CL & Fenton MA 1937. Belt Series of the north: stratigraphy, sedimentation, paleontology. Geological Society of America Bulletin 48: 1873–1970.

Food and Agriculture Organization 1974. Soil map of the world, v. I. Legend. Paris, UNESCO, Paris, 59 p.

Frey SE, Gingras MK & Dashtgard SE 2009. Experimental studies of gas–escape and water escape structures: mechanisms and morphologies. Journal of Sedimentary Research 79: 808–816.

Fritsche A 1908. Problematica Silurica. *In*: Barrande O (Editor)─ Système Silurien du Centre de la Bohème. Prague, R. Gerhard, 28 p.

Garcia–Pichel F & Wojciechowski MF 2009. The evolution of a capacity to build supra–cellular ropes enabled filamentous cyanobacteria to colonize highly erodible substrates. PloS One 4: e7801–1–6.

Gaidos E, Dubuc T, Dunford M, McAndrew F, Padilla–Gamiño J, Studer B,

Weersing K & Stanley S 2007. The Precambrian emergence of animal life: a geobiological perspective. Geobiology 5: 351–373.

Gnilovskaya MB 1985. Vendian actinomycetes and organisms of uncertain systematic position. *In*: Sokolov BS & Iwanowski AB (Editors)─The Vendian System: Vol. 1 Paleontology. Berlin, Springer: 148–153.

Gold DA 2018. The slow rise of complex life as revealed through biomarker genetics. Emerg. Topics Life Science 2: 191–199.

Graham LE, Wilcox LW & Graham JM 2009. Algae. San Francisco, Cummings, 420 p.

Hallbauer DK, Jahns HM & Beltmann HA 1977. Morphological and anatomical observations on some Precambrian plants from the Witwatersrand, South Africa. Geologische Rundschau 66: 477–491.

Häntzschel W 1975. Treatise on invertebrate paleontology. Part. W. Miscellanea. Supplement 1. Trace fossils and problematica. Boulder and Lawrence, Geol. Soc. America and Univ. Kansas Press, 269 p.

Hermann TN & Podkovryov VN 2006. Fungal remains from the Late Riphean. Paleontological Journal 40: 207–214.

Hofmann HJ 1971. Precambrian fossils, pseudofossils and Problematica in Canada. Geological Survey of Canada Bulletin 189: 1–146.

Hofmann HJ 1991a. Megascopic dubiofossils. *In*: Schopf JW & Klein C (Editors)─The Proterozoic biosphere: a multidisciplinary study. Cambridge, Cambridge University Press: 413–419.

Hofmann HJ 1991b. Proterozoic and selected Cambrian megascopic carbonaceous films. *In*: Schopf JW & Klein C (Editors)─The Proterozoic biosphere: a multidisciplinary study. Cambridge, Cambridge University Press: 957–979.

Homann M, Heubeck C, Airo A & Tice MM 2015. Morphological adaptations of 3.22 Ga–old tufted microbial mats to Archean coastal habitats (Moodies Group, Barberton Greenstone Belt, South Africa). Precambrian Research 266: 47–64.

Houston RS, Karlstrom KE, Graff PE, & Flurkey AJ 1992. New stratigraphic subdivisions of Late Archean and Early Proterozoic metasedimentary and metavolcanic rocks of the Sierra Madre and Medicine Bow Mountains, southern Wyoming. U.S. Geological Survey Professional Paper 1520: 1–50.

Hu C–X, Liu Y–D, Song L–R & Zhang DL 2002. Effect of desert soil algae on the stabilization of fine sands. Journal of Applied Phycology14: 281–292.

Hu J–M 1997. Vermiform trace fossils from the Precambrian Ruyang Group, western Henan. Chinese Science Bulletin 42: 251–254.

Huldtgren T, Cunningham JA, Yin C, Stampanoni M, Marone F, Donoghue PCJ, & Bengtson S 2011. Fossilised nuclei and germinating structures identify Ediacaran "animal embryos" as encysting protists. Science 334: 1696–1699.

Jennings DS & Driese SG 2014. Understanding barite and gypsum precipitation in upland acid–sulfate soils: An example from a Lufkin Series toposequence, south–central Texas, USA. Sedimentar Geology 299: 106–118.

Jones DS, Snoke AW, Premo WR & Chamberlain KR 2010. New models for Palaeoproterozoic orogenesis in the Cheyenne Belt region: evidence from the geology and U–Pb geochronology of the Big Creek Gneiss, southwestern Wyoming. Geological Society of America Bulletin 122: 1877–1898.

Karlstrom KE, Flurkey AK & Houston RS 1983. Stratigraphy and depositional setting of the Proterozoic Snowy Pass Supergroup, southeastern Wyoming: record of an early Proterozoic Atlantic–type cratonic margin. Geological Society of America Bulletin 94: 1257–1274.

Kauffman EG & Steidtmann JR 1981. Are these the oldest metazoan trace fossils? Journal of Paleontology 55: 923–947.

Kauffman EG, Elswick ER, Johnson CC & Chamberlain K 2009. The first diversification of metazoan life: biogeochemistry and comparative morphology of 1.9–2.5 billion year old trace fossils to Phanerozoic counterparts. 9th North American Paleontological Convention Proceedings of the Cincinnati Museum Center Science Contribution 3: 62.

Kennedy M, Droser M, Mayer LM, Pevear D & Mrofka D 2006. Late Precambrian oxygenation; inception of the clay mineral factory. Science 311: 1446–1449.

Kirschvink JL & Kopp RE 2008. Palaeoproterozoic ice houses and the evolution of oxygen–mediating enzymes: the case for a late origin of photosystem II. Royal Society of London Philosophical Transactions 363: 2755–2765.

Knauth LP & Kennedy MJ 2009. The late Precambrian greening of the Earth. Nature 460: 728–732.

Komar PD & McManus J 1999. Natural tracers of coastal sediments. *In*: Ewing L, Magoon OT & Robertson S (Editors)─Sand rights '99; bringing back the beaches. American Society of Civil Engineers Conference Proceedings: 70–84.

Lignier O 1906. *Radiculites reticulatus*, radicelle fossile de Sequoinee. Societé Botanique du France Bulletin 6: 193–201.

Loron CC, François C, Rainbird RH, Turner EC, Borensztajn S & Javaux EJ 2019. Early fungi from the Proterozoic era in Arctic Canada. Nature 570: 232−235.

MacRae C 1999. Life etched in stone: fossils of South Africa. Johannesburg, Geological Society of South Africa, 305 p.

Maloof AC, Rose CV, Beach R, Samuels BM, Calmet CC, Erwin DH, Poirier GR, Yao N & Simons FJ 2010. Possible animal–body fossils in pre–Marinoan limestones from South Australia. Nature Geoscience 3: 653–659.

Maloof AC, Porter SM, Moore JL, Dudás FÖ, Bowring SA, Higgins JA, Fike DA & Eddy MP 2011. The earliest Cambrian record of animals and ocean geochemical change. Geological Society of America Bulletin 122: 1731–1774.

Matz MV, Frank TM, Marshall NJ, Widder EA & Johnsen S 2008. Giant deep–sea protist produces bilaterian–like traces. Current Biology 18: 1849−1854.

Maynard JB 1992. Chemistry of modern soils as a guide to interpreting Precambrian fossil soils. Journal of Geology 100: 279–289.

Meert JG, Gibsher AS, Levashova NM, Grice WC, Kamenov GD & Ryabinin AB 2011. Glaciation and ~770Ma Ediacara (?) Fossils from the Lesser Karatau Microcontinent, Kazakhstan. Gondwana Research 19: 867–880.

Mihail JD & Bruhn JN 2005. Foraging behaviour of *Armillaria* rhizomorph systems. Mycological Research 109: 1195–1207.

Minter WE 2006. The sedimentary setting of Witwatersrand placer mineral deposits in an Archean atmosphere. *In*: Kesler SE & Ohmoto H (Editors)─Evolution of early Earth's atmosphere, hydrosphere, and biosphere; constraints from ore deposits. Geological Society of America Memoir 198: 105–119.

Mitchell RL & Sheldon ND 2009. Weathering and paleosol formation in the 1.1 Ga Keweenawan Rift. Precambrian Research 168: 271–283.

Mossman DJ & Farrow CEG 1992. Paleosol and ore–forming processes in the Elliot Lake District of Canada. *In*: Schidlowski M, Golubic S, Kimberley MM, McKirdy DM & Trudinger PA (Editors)─Early organic evolution: implications for mineral and energy resources. Berlin, Springer: 67–75.

Mossman DJ, Minter WEL, Dutkiewicz A, Hallbauer DK, George SC, Hennigh Q, Reimer TO & Horscroft FD 2008. The indigenous origin of Witwatersrand 'carbon'. Precambrian Research 164: 173–186.

Mueller GM, Bills GF & Foster MS 2004. Biodiversity of Fungi. Amsterdam, Elsevier, 777 p.

Nabhan S, Luber T, Scheffler T & Heubeck C 2016. Climatic and geochemical implications of Archean pedogenic gypsum in the Moodies Group (~3.2 Ga), Barberton Greenstone Belt, South Africa. Precambrian Research 275: 119–134.

Narbonne GM, Kaufman AJ & Knoll AH 1994. Integrated chemostratigraphy and biostratigraphy of the Windermere Supergroup, northwest Canada; implications for Neoproterozoic correlations and the early evolution of animals. Geological Society of America Bulletin 106: 1281–1292.

Navarro–González R, Rainey FA, Molina P, Bagalay DR, Hollen BJ, de la Rosa J, Small AM, Quinn RC, Grunthaner FJ, Caceres I, Gomez–Silva B & McKay CP 2003. Mars–like soils in the Atacama Desert, Chile, and the dry limit of microbial life. Science 302: 1018–1021.

Neuweiler F, Turner EC & Burdige DJ 2009. Early Neoproterozoic origin of the metazoan clade recorded in carbonate rock texture. Geology 37: 475–478.

Nishida N, Pigg KB, Kudo K & Rigby JF 2007. New evidence of reproductive organs of Glossopteris based on permineralized fossils from Queensland, Australia. I. Ovulate organ *Homevaleia* gen. nov. Journal of Plant Research 120: 539–549.

Niu SW 1997. The first discovery of the genus *Dickinsonia* (worm) in China. Tianjin Institute of Geology and Mineral Resources 20: 50–55. http: // en.cnki.com.cn/Article_en/CJFDTotal–QHWJ199703005.htm

Noffke N 2007. Microbially–induced sedimentary structures in Archean sandstones; a new window into early life. Gondwana Research 11: 336–342.

Noffke N, Eriksson KA, Hazen RM & Simpson EL 2006. A new window into early Archean life; microbial mats in Earth's oldest siliciclastic tidal deposits (3.2 Ga Moodies Group, South Africa). Geology 34: 253–256.

Peterson KJ, Waggoner B & Hagadorn JW 2003. A fungal analog for Newfoundland Ediacaran fossils? Integrative and Comparative Biology 43: 127–136. https: //doi.org/10.1093/icb/43.1.127

Piper JDA 2010. Protopangaea: palaeomagnetic definition of Earth's oldest (mid–Archaean–Palaeoproterozoic) supercontinent. Journal of Geodynamics 50: 154–165.

Planavsky N, Neuweiler F, Turner EC & Burdige DJ 2009. Early Neoproterozoic origin of the metazoan clade recorded in carbonate rock texture; discussion and reply. Geology 37: e195–e197.

Poelt, J & Baumgärtner H 1964. Über Rhizinenstränge bei placodialen Flechten. Österreichen Botanische Zeitschrift 111: 1–18.

Potonié H 1893. Die Flora des Rotliegenden von Thüringen. Prüssische Geologisches Landestalt Abhandlungen 9: 1–298.

Prashnowsky AA & Schidlowski M 1967. Investigation of a Precambrian thucolite. Nature 216: 560–563.

Rasmussen B & Muhling JR 2007. Monazite begets monazite: evidence for dissolution of detrital monazite and reprecipitation of syntectonic monazite during low–grade regional metamorphism. Contributions to Mineralogy and Petrology 154: 675–689.

Rasmussen B, Bose PK, Sarkar S, Banerjee S, Fletcher IR & McNaughton NJ 2002. 1.6 Ga U–Pb zircon age for the *Chorhat* Sandstone, lower Vindhyan, India; possible implications for early evolution of animals. Geology 30: 103–106.

Rasmussen B, Blake TS, Fletcher IR & Kilburn MR 2009. Evidence for microbial life in synsedimentary cavities from 2.75 Ga terrestrial environments. Geology 37: 423–426.

Ray JS, Martin MW, Veizer J & Bowring SA 2002. U–Pb zircon dating and Sr isotope systematics of the Vindhyan Supergroup, India. Geology 30: 131–134.

Retallack GJ 1983. Late Eocene and Oligocene paleosols from Badlands National Park, South Dakota. Geological Society of America Special Paper 193: 1–82.

Retallack GJ 1991. Miocene paleosols and ape habitats from Pakistan and Kenya. New York, Oxford Univ. Press, 175 p.

Retallack GJ 1992. What to call early plant formations on land. Palaios 7: 508–520.

Retallack GJ 1997. A colour guide to paleosols. Chichester, Wiley, 346 p.

Retallack GJ 2007. Decay, growth, and burial compaction of *Dickinsonia*, an iconic Ediacaran fossil. Alcheringa 31: 215–240.

Retallack GJ 2008. Cambrian palaeosols and landscapes of South Australia. Australian Journal of Earth Sciences 55: 1083–1106.

Retallack GJ 2009a. Cambrian–Ordovician non–marine fossils from South Australia. Alcheringa 33: 355–391.

Retallack GJ 2009b. Early Paleozoic pedostratigraphy and global events in Australia. Australian Journal of Earth Sciences 56: 569–584.

Retallack GJ 2011a. Neoproterozoic glacial loess and limits to snowball Earth. Journal of the Geological Society of London 168: 1–19.

Retallack GJ 2011b. Problematic megafossils in Cambrian palaeosols of South Australia. Palaeontology 54: 1223–1242.

Retallack GJ 2012a. Criteria for distinguishing microbial mats and earths. *In*: Noffke N & Chafetz H (Editors)─Microbial mats in siliciclastic sediments. Society of Economic Paleontologists and Mineralogists Special Paper 101: 136–152.

Retallack GJ 2012b. Were Ediacaran siliciclastics of South Australia shallow or deep marine? Sedimentology 59: 1208–1236.

Retallack GJ 2013. Comment on "Trace fossil evidence for Ediacaran bilaterian animals with complex behaviors" by Chen *et al.* [Precambrian Res. 224 (2013) 690–701]. Precambrian Research 231: 383–385.

Retallack GJ 2015a. Reassessment of the Silurian problematicum *Rutgersella* as another post–Ediacaran vendobiont. Alcheringa 39: 573–588.

Retallack GJ 2015b. Acritarch evidence of a late Precambrian adaptive radiation of Fungi. Botanica Pacifica 4(2): 19−33

Retallack GJ 2018. Oldest recognized palaeosol profiles on Earth, Panorama Formation (3.46 Ga), Western Australia. Palaeogeography Palaeoclimatology Palaeoecology 489: 230–248.

Retallack GJ 2020. Zebra rock and other Ediacaran paleosols in Western Australia. Australian Journal of Earth Sciences (in press) https: //doi.org /10.1080/08120099.2020.1820574.

Retallack GJ & Dilcher DL 1988. Reconstructions of selected seed ferns. Annals of the Missouri Botanical Garden 75: 1010–1057.

Retallack GJ & Kirby MX 2007. Middle Miocene global change and paleogeography of Panama. Palaios 22: 667–679.

Retallack GJ & Mao X–G 2019. Palaeoproterozoic (ca. 1.9 Ga) megascopic life on land in Western Australia. Palaeogeography Palaeoclimatology Palaeoecology 532: 109266.

Retallack GJ & Mindszenty A 1994. Well preserved Late Precambrian palaeosols from northwest Scotland. Journal of Sedimentary Research A64: 264–281.

Retallack GJ, Krull ES & Bockheim JG 2001. New grounds for reassessing paleoclimate of the Sirius Group, Antarctica. Journal of the Geological Society of London 158: 925–635.

Retallack GJ, Dunn KL & Saxby J 2013a. Problematic Mesoproterozoic fossil *Horodyskia* from Glacier National Park, Montana, USA. Precambrian Research 226: 125–142.

Retallack GJ, Krull ES, Thackray GD & Parkinson D 2013b. Problematic urn–shaped fossils from a Palaeoproterozoic (2.2 Ga) palaeosol in South Africa. Precambrian Research 235: 71–87.

Retallack GJ, Krinsley DH, Fischer R, Razink JJ & Langworthy K 2016. Archean coastal–plain palaeosols and life on land. Gondwana Research 40: 1–20.

Riksen MJPM & Goossens D 2007. The role of wind and splash erosion in inland drift–sand areas in the Netherlands. Geomorphology 88: 179–192.

Runnegar BN 1991. Proterozoic fossils of soft–bodied metazoans (Ediacara faunas). *In*: Schopf JW & Klein C (Editors) ─The Proterozoic biosphere: a multidisciplinary study. Cambridge, Cambridge University Press: 999–1007.

Runnegar BN & Fedonkin MA 1991. Proterozoic metazoan body fossils. *In*: Schopf JW & Klein C (Editors)─The Proterozoic biosphere: a multidisciplinary study. Cambridge, Cambridge University Press: 369–388.

Rye R & Holland HD 1998. Paleosols and the evolution of atmospheric oxygen; a critical review. American Journal of Science 298: 621–672. https: //doi.org/10.2475/ajs.298.8.621

Rye R & Holland HD 2000. Life associated with a 2.76 Ga ephemeral pond? Evidence from Mount Roe #2 paleosol. Geology 28: 483–486.

Sadler PM 1981. Sediment accumulation rates and the completeness of stratigraphic sections. Journal of Geology 89: 569–584.

Sawada H, Isozaki Y, Sakata S, Hirata T & Maruyama S 2018. Secular change in lifetime of granitic crust and the continental growth: A new view from detrital zircon ages of sandstones. Geoscience Frontiers 9: 1099–1115.

Schiffbauer JD, Huntley JW, O'Neil GR, Darroch SA, Laflamme M & Cai Y 2016. The latest Ediacaran Wormworld fauna: setting the ecological stage for the Cambrian Explosion. GSA Today 26: 4–11.

Schopf JW & Packer BM 1987. Early Archean (3.3–billion to 3.5–billion–year–old) microfossils from Warrawoona Group, Australia. Science 237: 70–73.

Seilacher A 2007. Trace fossil analysis. Berlin, Springer, 226 p.

Seilacher A, Bose PK & Pflüger F 1998. Triploblastic animals more than 1 billion years ago; trace fossil evidence from India. Science 282: 80–83.

Serezhnikova EA, Ragozina AL, Dorjnamjaa D & Lyubov VZ 2014. Fossil microbial communities in Neoproterozoic interglacial rocks, Maikhanuul Formation, Zavkhan basin, Western Mongolia. Precambrian Research 245: 66–79.

Sergeev VN 2009. The distribution of microfossil assemblages in Proterozoic rocks. Precambrian Research 173: 212–222.

Shapiro JA 1998. Thinking about bacterial populations as multicellular organisms. Annual Review of Microbiology 52: 81–104.

Sheldon ND & Retallack GJ 2001. Equation for compaction of paleosols due to burial. Geology 29: 247–250.

Sheldon ND & Tabor NJ 2009. Quantitative paleoenvironmental and paleoclimatic reconstruction using palaeosols. Earth Science Reviews 95: 1–52.

Sheldon ND, Retallack GJ & Tanaka S 2002. Geochemical climofunctions from North American soils and application to palaeosols across the Eocene–Oligocene boundary in Oregon. Journal of Geology 110: 687–696.

Simpson EL, Heness E, Bumby A, Eriksson PG, Eriksson KA, Hilbert–Wolf HL, Linnevelt S, Malenda HF, Modungwa T & Okafor OJ 2013. Evidence for 2.0 Ga continental microbial mats in a paleodesert setting. Precambrian Research 237: 36–50.

Soil Survey Staff 2014. Keys to Soil Taxonomy. Washington DC, Natural Resources Conservation Service, 358 p.

Stephenson SI & Stempen H 1994. Myxomycetes: a handbook of slime molds. Portland, Timber Press, 200 p.

Terry RD & Chilingar GV 1955. Summary of "Concerning some additional aids in studying sedimentary formations" by M.S. Shvetsov. Journal of Sedimentary Petrology 25: 229–234.

Thompson JB 1972. Oxides and sulfides in regional metamorphism of pelitic schists. Proceedings of 24th International Geological Congress Montreal 10: 27–35.

Traverse A 1988. Paleopalynology. London, Unwin Hyman, 600 p.

Turland NJ, Wiersema JH, Barrie FR, Greuter W, Hawksworth DL, Herendeen PS, Knapp S, Kusber WH, Li DZ, Marhold K & May TW 2018. International Code of Nomenclature for algae, fungi, and plants (Shenzhen Code) adopted by the Nineteenth International Botanical Congress Shenzhen, China, July 2017. Regnum Vegetabile 159: 1–254.

Vahrenkamp VC, Rossinsky V, Knauth LP & Beeunas MA 1987. Preserved isotopic signature of subaerial diagenesis in the Mescal Limestone, central Arizona: discussion and reply. Geological Society of America Bulletin 99: 595–597.

Watanabe Y, Martini JE & Ohmoto H 2000. Geochemical evidence for terrestrial ecosystems 2.6 billion years ago. Nature 408: 574−578.

Watanabe Y, Stewart BW & Ohmoto H 2004. Organic–and carbonate–rich soil formation approximately 2.6 billion years ago at Schagen, east Transvaal District, South Africa. Geochimica Cosmochimica Acta, 68: 2129–2151.

Williams GE & Schmidt PW 2003. Possible fossil impression in sandstone from the late Palaeoproterozoic–early Mesoproterozoic Semri Group (lower Vindhyan Supergroup), central India. Alcheringa 27: 75–76.

Yaalon DH, Moshe R & Nissim S 1982. Evolution of reg soils in southern Israel and Sinai. Geoderma 28: 173–202.

Yakimenko E, Inosemtsev S & Naugolnykh S 2004. Upper Permian palaeosols (Salarevskian Formation) in the central part of the Russian Platform: paleoecology and paleoenvironment. Revista Mexicana Ciencias Geologicas 21: 111–119.

Yang SP & Zhou HR 1995. Trace fossils from the Precambrian Ruyang Group of western Henan. Di zhi lun ping (Geological Review) 41: 205−210.

Zhang X–L, Hua H & Reitner J 2006. A new type of Precambrian megascopic fossils: the Jinxian biota from northeastern China. Facies 52: 169–181.

Zhang X–L, Shu DG & Erwin DH 2007. Cambrian naraoiids (Arthropoda); morphology, ontogeny, systematics, and evolutionary relationships. Journal of Paleontology 81(issue 5, supplement): 1–52.

Ziegenbalg SB, Brunner B, Rouchy JM, Birgel D, Pierre C, Boettcher ME, Caruso A, Immenhauser A & Peckmann J 2010. Formation of secondary carbonates and native sulphur in sulphate–rich Messinian strata, Sicily. Sedimentar Geology 227: 37–50.